

3-31-2016


MENs Doped Adhesive and Influence on Fracture Toughness

Kao Z. Yang

Florida International University, kyang006@fiu.edu

DOI: 10.25148/etd.FIDC000238

Follow this and additional works at: <https://digitalcommons.fiu.edu/etd>

 Part of the [Aerospace Engineering Commons](#), [Aviation Commons](#), [Electrical and Computer Engineering Commons](#), [Materials Science and Engineering Commons](#), and the [Mechanical Engineering Commons](#)

Recommended Citation

Yang, Kao Z., "MENs Doped Adhesive and Influence on Fracture Toughness" (2016). *FIU Electronic Theses and Dissertations*. 2487.
<https://digitalcommons.fiu.edu/etd/2487>

This work is brought to you for free and open access by the University Graduate School at FIU Digital Commons. It has been accepted for inclusion in FIU Electronic Theses and Dissertations by an authorized administrator of FIU Digital Commons. For more information, please contact dcc@fiu.edu.

FLORIDA INTERNATIONAL UNIVERSITY

Miami, Florida

MENS DOPED ADHESIVE AND INFLUENCE ON FRACTURE TOUGHNESS

A thesis submitted in partial fulfillment of the
requirements for the degree of

MASTER OF SCIENCE

in

MATERIALS SCIENCE AND ENGINEERING

by

Kao Zoua Yang

2016

To: Interim Dean Ranu Jung
College of Engineering and Computing

This thesis, written by Kao Zoua Yang, and entitled MENs Doped Adhesive and Influence on Fracture Toughness, having been approved in respect to style and intellectual content, is referred to you for judgment.

We have read this thesis and recommend that it be approved.

Dwayne McDaniel

Sakhrat Khizroev

Benjamin Boesl, Major Professor

Date of Defense: March 31, 2016

The thesis of Kao Zoua Yang is approved.

Interim Dean Ranu Jung
College of Engineering and Computing

Andrés G. Gil
Vice President for Research and Economic Development
and Dean of the University Graduate School

Florida International University, 2016

DEDICATION

I dedicate this thesis to my family. My parents were always there giving moral support and from times financial support. Without them the project and accomplishments would not be where they are today.

ACKNOWLEDGMENTS

I would like to acknowledge and thank the committee members of the thesis. Dr. Benjamin Boesl is a great adviser and mentor who gave tremendous support in the research and thesis, the research and thesis could not have been completed without him. Additionally Dr. Dwayne McDaniel and Dr. Sakhrat Khizroev provided tremendous support which was crucial in the research project. I would also like to acknowledge and thank all my peers, Dillon Watring, Jorge Coria and Vishal Musaramthota for their endless support in the research. I would also like to take the time to acknowledge and thank my previous advisers back in Eau Claire, WI. Dr. Patricia Quinn and Dr. Marcus McEllistrem provided great moral support during my time as a master's student and in times of need their support helped me through rough times Finally I would like to acknowledge and thank the FIU McNair Program for providing a financial support in everyday living expenses. Their generous support has given me the opportunity to succeed here at FIU.

ABSTRACT OF THE THESIS

MENS DOPED ADHESIVE AND INFLUENCE ON FRACTURE TOUGHNESS

by

Kao Zoua Yang

Florida International University, 2016

Miami, Florida

Professor Benjamin Boesl, Major Professor

Composites are in high demand; however, fasteners are often required for joining process and can reduce their advantages. One solution is adhesive bonding, but uncertainty exists regarding long term durability and the ability to interrogate bonds noninvasively. One potential solution to qualify bond integrity over its service life is to dope an adhesive with magneto-electric nanoparticles (MENS). MENS can yield output magnetic signatures that are influenced by bond quality and damage state. In this study, adhesives have been doped with MENS prior to bonding at 1% volume concentration. For optimum implementation, this health monitoring system should be evaluated for effects of the MENS on the mechanical properties. Lap-shear testing was conducted to assess changes in the bond strength from addition of the nanoparticles. End-notched flexure (ENF) tests were also conducted for fracture mechanism evaluation. Results showed an increase of 12% in shear strength as a function of MENS loading concentration. In addition, a feasibility study of output magnetic signature as a function of elevated temperature and humidity were evaluated for MENS doped and un-doped adhesives. Results gave an order of magnitude change in magnetic signal as a function of exposure time.

TABLE OF CONTENTS

CHAPTER	PAGE
I. INTRODUCTION	1
MOTIVATION	1
OBJECTIVE	4
II. LITERATURE REVIEW	6
MAGNETO-ELECTRIC NANOPARTICLES (MENS)	6
REVIEW OF FRACTURE OF ADHESIVES	10
MODES OF TESTING	15
LAP-SHEAR TESTING	18
III. METHODOLOGY	20
MATERIALS SELECTION	20
DISPERSION OF MENS	21
ASSESSMENT OF DISPERSION	22
BOND LINE MEASURING	22
LAP-SHEAR MANUFACTURING AND TESTING	24
ASSESSMENT OF LAP-SHEAR TESTING	25
ENF MANUFACTURING AND TESTING	26
ASSESSMENT OF ENF TESTING	27
ADHESIVE SCANNING	27
IV. RESULTS	29
BOND LINE MEASUREMENTS	29
UN-DOPED LAP-SHEAR RESULTS	32
DOPED LAP-SHEAR RESULTS	33
UN-DOPED AND DOPED LAP-SHEAR COMPARISON	34
UN-DOPED ENF GII RESULTS	36
DOPED ENF GII RESULTS	38
UN-DOPED AND DOPED ENF COMPARISON	40
IN-SITU ENF RESULTS	42
VIBRATING SCANNING MAGNETOMETRY RESULTS	43
V. DISCUSSION	46
RESEARCH CHALLENGES	46
APPLICATIONS	47
FURTHER WORK	47
SUMMARY	48
REFERENCES	49

LIST OF TABLES

TABLE	PAGE
Table 1. Materials used in Study	21
Table 2. Average Bond Line Measurements of Un-doped Lap-Shear	30
Table 3. Average Bond Line Measurements of Doped 1 vol. % Lap-Shear	30
Table 4. Average Bond Line Measurements of Un-doped ENF Samples	32
Table 5. Average Bond Line Measurements of Doped 1 vol. % ENF Samples	32
Table 6. Un-doped Lap-Shear Peak Load/Stress	33
Table 7. Doped Samples 1 vol. % Peak Load/Stress	34
Table 8. Dimensions and Crack Measurements of ENF Un-doped Samples	37
Table 9. G_{II} Values of Un-doped samples with Load/Displacement	37
Table 10. Dimensions and Crack Measurements of ENF Doped Samples	39
Table 11. G_{II} Values of Doped samples with Load/Displacement	39

LIST OF FIGURES

FIGURE	PAGE
1. 787 Boeing Dreamliner Airplane	2
2. Mechanical Fastener Joining Two Composite Plates	3
3. TEM Characterization of MENs	6
4. Magnetic Signatures of MENs with Different Surface Charge Densities	7
5. Typical Failure Modes of Adhesives	12
6. Three Different Types of Loading. a) Mode-I, b) Mode-II, c) Mode-III	14
7. DCB Sample Setup	15
8. ENF Fixture and Sample Loading Diagram	16
9. ENF Fixture for In-situ SEM/FIB	16
10. Mix Mode Sample Setup	18
11. MTS Criterion Model 43	19
12. Lap-shear Sample Dimensions	19
13. D-spacing for CoFe_2O_4 with 2.1 Angstroms	22
14. Bond Line Measurement of Lap-Shear Sample	24
15. Lap-shear Sample Configuration for MTS Criterion Model 43	25
16. Spacer Cutouts to be placed on Top of the Laminate	27
17. Bond Line Measurements of Lap-Shear Un-doped	29
18. Bond Line Measurements of Lap-Shear Doped	30
19. Bond Line Measurement of ENF Un-doped	31
20. Bond Line Measurement of ENF Doped	32
21. Load vs. Displacement Graph of Un-doped 1 vol. % Lap-Shear	33

22. Load vs. Displacement Graph of Doped 1 vol. % Lap-Shear	34
23. Averages of the Peak Load for Lap-Shear Comparisons	35
24. Averages of the Peak Stress for Lap-Shear Comparisons	36
25. Load Displacement Graph of Un-doped ENF Samples	38
26. Load Displacement Graph of Doped ENF Samples	40
27. Un-doped and Doped ENF Comparisons	41
28. Un-doped Before and After Loading In-Situ	42
29. Doped Before and After Loading In-Situ	42
30. Magnetic Signatures of Un-doped and Doped Baselines	44
31. Magnetic Signature of Doped Baseline and environmental Exposed Doped	44
32. Magnetic Signatures of Out of Plane/In Plane E.E. Doped and UV	45

CHAPTER I – INTRODUCTION

Composites are a combination of two or more materials that have different properties, but when combined they exhibit a mixture of both properties to an extent. For example, carbon fiber has a high strength to weight ratio of 3033.15 MPa/(g/cm³) compared to aluminum's 114.81 MPa/(g/cm³) [1,2]. Carbon fiber provides a stronger mechanical property choice at a lower density over conventional metals and ceramics. Composites are heavily used in aerospace and military applications, such as aircraft structures, military vehicle, and infantry armor. Although there are many different types of composites, the material of primary interest is carbon fiber reinforced plastic (CFRP). A current challenge presented in adhesive bonding is that there is no guaranteed technique to qualify the strength of the bond over its lifetime. Although fasteners do provide a known failure path, the benefit does not necessarily outweigh the use of pure adhesive bonding. Creating a multi-functional adhesive by doping it with magneto-electric nanoparticles (MENs) can be a solution. MENs as a dopant can be used to increase the strength of the adhesive while providing a structural health monitoring (SHM) capability to evaluate bond integrity. The introduction to environmental exposure and mechanical loading is expected to have different magnetic signatures than baseline which serves as the fundamental of the SHM.

MOTIVATION

Composites are used virtually everywhere now. The most known and publicized use of composites is the new Boeing 787 Dreamliner (figure 1) airplane. The entire fuselage was constructed out of a one piece composite. Other advantages that composites provide are corrosion resistance, robust design and electrical insulating properties. A

current state of the art procedure in using composites for aircraft structures is to incorporate mechanical fasteners to join composite panels (figure 2). A benefit of using mechanical fasteners is that it provides a known secondary load path for the fracture to occur. However; its benefit does not necessarily outweigh the disadvantages. Disadvantages of mechanical fasteners include added additional weight and materials cost, stress concentrations from drilled holes, higher stress intensity after repairs, and more inspection points [3].



Figure 1. 787 Boeing Dreamliner Airplane, retrieved from <http://www.boeing.com/commercial/787/>



Figure 2. Mechanical Fastener Joining Two Composite Plates, retrieved from <http://www.assemblymag.com/articles/90348-aerospace-fastening-in-the-21st-century>

A proposed solution to mechanical fasteners is to incorporate pure adhesive bonding across the entire panel. Adhesive bonding can provide many solutions to the disadvantages of mechanical fasteners. However; due to the inability to qualify bonds over their lifetime, adhesive bonding alone in primary structures presents a problem. To counter this dilemma, MENs will be used as a dopant in the adhesive. By doping the adhesive with MENs, it can serve as a multi-functional adhesive as a stronger adhesive and SHM system for the adhesive bond life. Over the life of the bond, it will be subjected to various mechanical loading and environmental exposures. Each of these conditions will introduce water ingress, micro-cracks and stress concentrations. The plan here is to correlate each specific damage state to a specific magnetic signature. This specific signature than can be used to compare with the baseline to determine the health state of the bond.

OBJECTIVE

The end goal of the research project is to understand the effects of MENs on the fracture properties and strength while providing a SHM component. SHM techniques are highly advantageous as they can non-invasively inspect structures. Typically stress-strain states of structures are monitored however with the introduction of MENs, bond health monitoring is possible. The overall research can be divided into two objectives: Objective 1 is the assessment of the mechanical strengthening of the adhesive by doping the adhesive. Objective 2 goals are to simulate environmental conditions and compare the magnetic signatures to a known baseline.

Objective 1 will be the main focus of the thesis. In order for the doped adhesive to be used as a viable multi-functional adhesive, it first must be prove that the addition of MENs does not adversely affect mechanical strength. Nanoparticles in general have been used as strengthening fillers and will provide the fundamental concept of strengthening the adhesive too. The adhesive will be doped at a small concentration of 1 vol. % and be tested on two scale levels. Micro-scale level testing will involve the use of end-notched flexure (ENF) testing which will be used to compare energy release rates (G_{II}) between un-doped and doped samples. In addition to the ENF tests, the samples will be loaded inside a focused ion beam-scanning electron microscope (FIB-SEM) for real time fracture/damage mechanisms. Macro-scale level testing will involve the use of single lap-shear testing in which the ultimate shear strength will be compared between un-doped and doped samples.

Objective 2 focuses on the comparison of magnetic signatures between doped samples and un-doped samples. Doped samples will include baseline doped,

environmental exposed doped and ultra-violet (UV) exposed doped. The magnetic signatures will be collected with a vibrating sample magnetometer (VSM). The goal here is to establish a baseline magnetic signature of the pure adhesive alone without MENs and compare it to the other doped and exposed doped sets. Un-doped and doped samples will be needed to compare the sensitivity of the MENs and determine if changes to concentration or diameter size of particles is necessary. The next step will introduce the doped samples to environmental conditions. To simulate environmental conditions, the samples will be placed in an environmental chamber that controls constant humidity and temperature control for a period of one month at 70°C and 95% relative humidity. In addition, a doped sample set will be introduced to UV radiation for one month. Finally the last task is to scan the all the sample sets and compare their signatures with the baseline and baseline doped samples. A change in the order of magnitude of the magnetic moment is used to determine the change in magnetic signature. The magnetic moment and applied field are measured and graphed. Depending on the conditions, the magnitude of the environmentally exposed samples should display orders of magnitude difference in the magnetic moment.

CHAPTER II – LITERATURE REVIEW

MAGNETO-ELECTRIC NANOPARTICLES (MENS)

Nanoparticles are particles that are on the order scale of nanometers (figure 3). For example, sand grains would be on the order scale of millimeters as they can range from 2mm up to 64mm. What makes MENS a special type of nanoparticles is the added effect known as the magneto-electric effect (ME). ME effect stated by Fiebig is “the coupling between electric and magnetic fields in matter” [4]. There are two main field effects that can be induced with the MENS. The first field effect is the magnetization of the MENS by inducing an electric field and the second field effect is electric polarization with induced magnetic field [5]. The ME effect is commonly found in ferrite composite materials that display ferromagnetism.

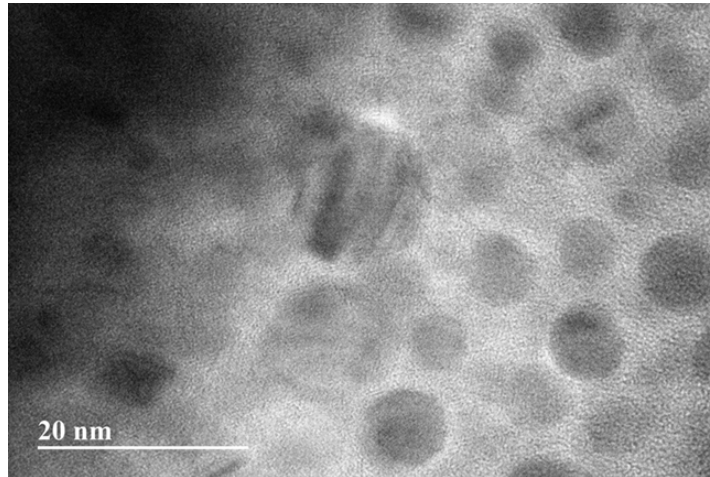


Figure 3. TEM Characterization of MENS

The current exploitation and significance of MENS is mainly due to the ME effect. The principle of reciprocity dictates that the ME effect is calculated as $\Delta P = \alpha H$, where α is the ME coefficient, and H is the induced electric field. Similarly, the dipole surface charge density on the MENS can be approximated as $\sigma_{ME} \approx \frac{Q}{\pi d^2}$ where Q is the

electric charge of the MENs and d is the diameter of the MENs. The charge density of the MENs can then be summed up as $\sigma_{ME} \approx \alpha H$. Rearranging the equations, we can solve for a theoretical induced electric field based on the different surface charge densities shown in the formula: $H_{th} \approx \frac{Q}{\pi d^2 \alpha}$. Figure 4 below portrays magnetic signatures of MENs with various surface densities. Magnetic signatures are obtained with VSM and other magnetometry techniques. The VSM measures the magnetic properties of magnetic materials. These properties can be then displayed in hysteresis loops, magnetization curves, and spectrums.

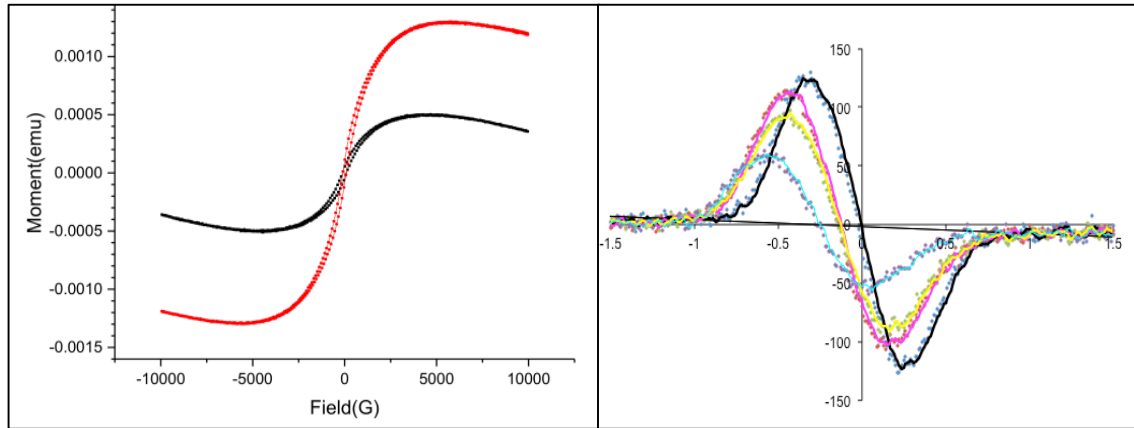


Figure 4. Magnetic Signatures of MENs with Different Surface Charge Densities

In the recent past, MENs has been used mainly in the applications of biomedicine. Because MENs can be manufactured in a size scale of a couple nanometers to hundreds of nanometers in diameter, they can interact with viruses, cells, proteins and even genes [6]. This allows MENs to be applied in the use of drug delivery systems. Khizroev's work in functionalizing the MENs has allowed the MENs to be bonded to a drug. The drug then can be selectively released by applying an external magnetic field [7]. More of Khizroev's work in MENs has also continued to use MENs as a non-invasive stimulus for

patients with Parkinson's disease and specific ovarian cancer cell target for drug delivery [8, 9]. Other applications outside of biomedicine include the use of BiFeO₃ MENs for photo catalysis and magnetic thin films using Ca₃CoMnO₆ MENs [10,11]. MENs have also been used in nano-composites for shape memory capabilities. Petcharoen and Sirivat's work exploited the magneto-electric effect of the particles by inducing an electric field to deflect the material in the direction of the field [12]. When the field was removed, the material was able to reform back to its normal state.

Another mechanism for MENs and nanoparticles is that it can provide a strengthening mechanism when used as a doping material in adhesives. Many studies have shown that material properties of adhesives can be increased with nanoparticle reinforcement. Studies done by Kinloch et al. developed a model and characterization of toughening epoxy based adhesives using silica nanoparticles [13, 14, 15]. The effects on particle size and load were also studied and fracture energy (G_c) was obtained for correlations. It is noted here that the particle load plays a critical role in the toughening mechanism. Starting at small concentrations, ~1 wt. % nanoparticles and higher, fracture toughness increases. However, there is a "plateau effect" with particle loading where the toughening effect is no longer effective after reaching a maximum concentration load. A study by Fu, Feng, Lauke, and Mai on calcium carbonate nanoparticles showed that concentrations greater than 30 vol. % to have no toughening effect and even start to decrease in toughness values in their system [16]. The optimum amount of particle load depends on the particle/resin selection and thus hard to quantify in a general sense. The loss in strengthening effect is due to the high surface activity of the nanoparticles. Because the particles are so small, their surface area to volume is high and makes them

highly prone to agglomerating. When the agglomerations become large due to high concentration loads, they can act as defects within the resin contributing to the lowering of strengthening values.

Additional research in nanoparticles reinforcement was studied with polyurethane foam and has shown improvements in properties. Uddin et al. study showed that by doping polyurethane foam with 3 wt. % of titanium dioxide (TiO_2), the polymer had superior ballistic performance in sandwich composites than before. The improvements were 20% more energy absorption and had lower residual velocity compared to un-doped composites [17]. Additionally, Mahfuz and Stewart's work in enhancing mechanical and fracture properties of sandwich composite using silicon carbide (SiC) particles has shown to improve the flexural properties by 50-70% and improvements to the energy release by 300% [18].

Silica nanoparticle reinforcement was also used as a dopant in epoxy resins. Friedrich et al. used 5 vol. % of 50nm particles to improve the elastic modulus, K_c and G_c by 200%, 70% and 140% respectively [19]. Mahrholz et al. looked at the outer limits of concentration of silica nanoparticles as dopants with 25 wt. % in epoxy resins. The results were in the improvements of the tensile modulus and flexural modulus by 36% and 30% respectively. Furthermore the tensile strength and flexural strength was improved by 11% and 9% respectively [20]. In addition to epoxy resins, a modified glass fiber reinforced epoxy composite (GFRP) was also looked at by Manjunatha et al. Silica nanoparticles were doped at 10 wt. % into an epoxy resin to make a GFRP composite. An improvement to the ultimate tensile strength and modulus for the epoxy resin was 19% and 17% respectively [21]. Another application of reinforcement is the use of aluminum

oxide (Al_2O_3) particles. Paramsothy et al. studied the reinforcement to a magnesium alloy ZK60A. They found improvements to the micro hardness, ultimate tensile strength, and tensile failure strain by 15%, 13% and 170% respectively [22].

As mentioned above, there is a well-established understanding of nanoparticle fillers and their effects as reinforcement. Their basis has provided the fundamentals needed to validate our study. The main criterion in our study is to introduce the MENs into our epoxy-based adhesive while maintaining no detrimental changes to the fracture properties. With understanding of how concentration loads effects properties, we can selectively choose better values that in theory should not affect the fracture properties and improve them. If we can successfully validate 1 vol. % doped MENs giving enhanced fracture properties in the adhesive compared to the un-doped, this technique can open door to the establishment of MENs incorporation into bonded adhesives systems.

REVIEW OF FRACTURE OF ADHESIVES

Historically adhesives were first used as sealants for ships. With early records dating back to 1500 BC, tar and jars of spices with asphalt were used [23]. Today adhesives are much more complex and are made both naturally and synthetically. Creton et al. describes adhesive not as a material type but in its function to bond two surfaces together [23]. There are many different types of adhesives each with their own specific applications. For example, epoxy based adhesives are used to bond CFRP as epoxy has a high chemical and temperature resistance compared to the other types of adhesives. This makes it a good choice in the automotive and aerospace industries. Other types of common adhesives are polyurethanes, polyimides and cyanoacrylates. Adhesives also come in various forms of physical states such as pastes and films. Paste adhesives usually

come in a two component batch, hardener and base. Once the hardener is mixed into the base, the curing will start and the adhesive will set. This is due to the crosslinking of long chains molecules which interlock the chains together.

There are two main concerns in adhesives that are considered when used; the glass transition temperature and adhesion strength. The glass transition temperature is the temperature at which the polymer chains of the adhesive start to loosen up making the adhesive more fluid like. If the operation temperatures are too high the life of the adhesive will degrade quickly. Adhesion strength is measured by the energy that is dissipated in a volume near the interface during crack propagation [23]. The adhesion strength or ability to bond will help determine fracture properties which are then considered in engineering design.

Today's technology allows for many types of bonding. Depending on the chemistry and situation, certain process of bonding can benefit over the other. Haisma et al. discussed the bonding basics and the different techniques used to bond surfaces together. Such as cold welding, fusion bonding, direct bonding, direct bonding + bond strengthening, silicon fusion bonding and UHV-bonding (ultra-high vacuum) [24]. Aside from the types of bonding, surface chemistry must also be considered to permit bonding. The three main types of surface chemistry that allow for surfaces to bond are forces, friction and mechanics. Forces can be attributed to chemical bonds such as Van Der Waals, hydrogen bonding and other chemical bonds. Mechanical bonding is used with fasteners which typically require an external part to create a joint between the two bonding surfaces. Frictional bonding happens when contact between the two surfaces are joined or "wield" through a frictional motion.

When a bonded surface experiences stress that exceeds the strength of the adhesive, it fails. Adhesives typically fail in two modes, adhesive failure and cohesive failure with a special third type of failure. Adhesive failure is when the adhesive fails, thus the adhesive layer and composite layer separates. Cohesive failure is when the fracture propagates within the adhesive layer. The third type of failure is when the composites itself fails which is highly undesirable. Figure 5 shows the graphical representation of how these failure modes appear. If the adhesive has strong bonding energy with the interface, cohesive failure will occur more favorably. However if the bonding of the adhesive with the interface is not sufficient due to contamination, surface chemistry, or surface texture, adhesive failure will most likely occur. Studies on cohesive failure on pressure sensitive adhesives (PSA) were performed to better understand and better express the energy associated with the failure which provides the first foundation knowledge of fracture mechanics in this study [25].

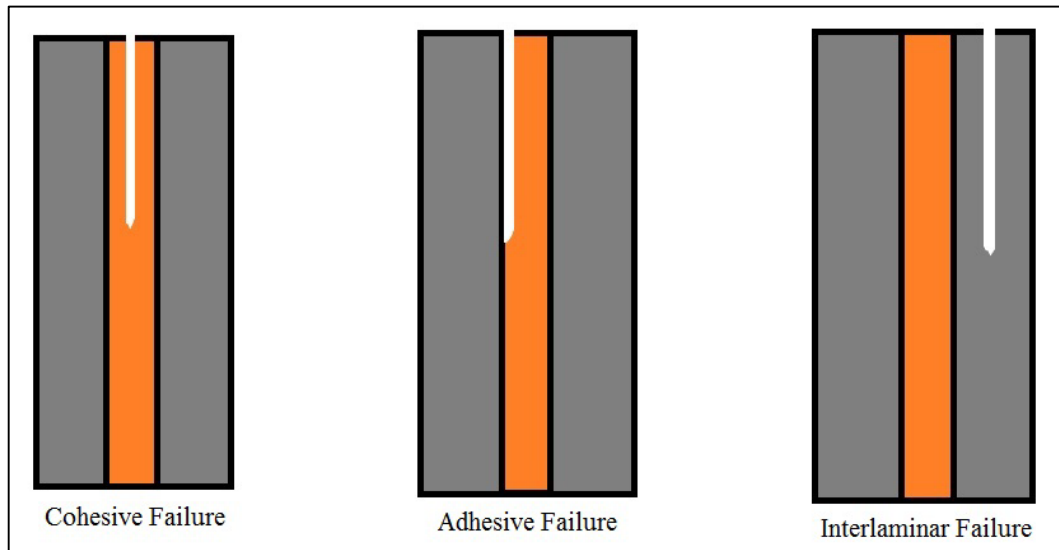


Figure 5. Typical Failure Modes of Adhesives

To determine the adhesive bonding strength, adhesives are bonded and broken to analyze the bond strength. Testing the adhesives is commonly done while they are bonded to a composite laminates or metal laminates. The fracture properties then can be gathered by the type of mode of testing. Fracture properties are often explained in as stress intensity factor (K) or strain energy release rate (G). K is used in fracture mechanics to define the stress state near the crack tip. When the crack propagates and extends, this is called the critical stress intensity factor which is denoted as K_c [26]. In testing, it is important to note the three loading types in testing K and G. These three loading types are categorized as Mode-I, Mode-II, and Mode-III. Referencing to figure 6 Mode-I corresponds to “a” where the load is applied in a tensile manner, Mode-II corresponds to “b” where the load is applied in a shear manner, and Mode-III corresponds to “c” where the load is applied with a tearing shear. Depending on the type of load we can also denote it as $K_{Ic}/K_{IIc}/K_{IIIc}$ with the Roman numeral indicating the type of mode. Similarly, G is related to K and has same notation. G indicates the amount of elastic energy the solid can sustain before propagating the crack. If the elastic energy is sufficient the crack propagates giving an increase in surface area and therefore an energy cost [26]. This can also be denoted as the critical energy release rate (CERR) or G_c [27]. The G_c can be further explained in the different types of loading in a similar manner to the K_c notation.

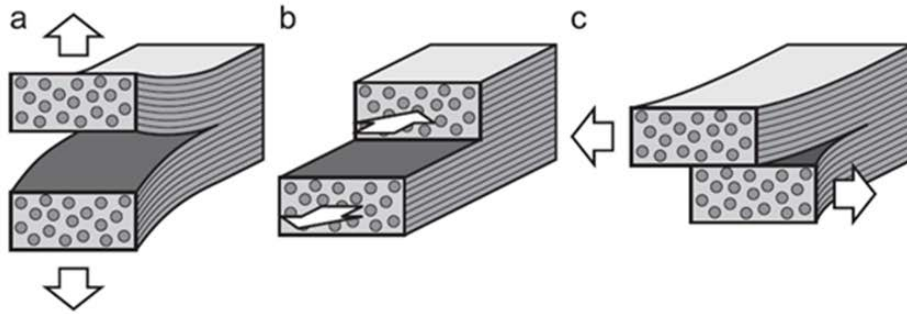


Figure 6. Three Different Types of Loading. a) Mode-I, b) Mode-II, c) Mode-III. Image retrieved from online journal: Adhesive joints in composite laminates—A combined numerical/ experimental estimate of critical energy release rates (fig. 2) by C. Balzani et al.

Another important factor that affects the K and G values is the bond line thickness. To maximize bonding strength, the bond line thickness needs to be optimized. A study by Silva et al. have looked upon three types of adhesive and how the bond line thickness relates back to the lap-shear strength [28]. The study consisted of three adhesives: Hysol EA 9361, Hysol EA 9321 and Araldite AV138/HV998. The Hysol adhesives were classified as a ductile adhesive and Araldite adhesive were classified as a brittle adhesive. The experiment consisted of testing the adhesives in a lap-shear configuration with bond line thickness of 0.2mm, 0.5mm and 1mm. From experimentation and modeling, they concluded that the lap-shear strength increases as the bond line thickness decreased from 1mm to an optimum value. Failure loads in kN of the adhesive at 0.2mm were 9.6, 11.1 and 12.5 compared to 1mm at 8.1, 8.2 and 10, respectively. Typically in adhesive bonding there is an optimal thickness that is recommended. Too large of a bond line thickness can alter the mechanical properties to

be more similar to the bulk (adhesive) and too little will not allow proper bonding between the adhesive and surface.

MODES OF TESTING

Mode I is commonly tested in a double cantilever beam test (DCB). Figure 7 displays a typical sample setup for DCB testing. In DCB testing, samples are typically manufactured with dimensions of 5" length with 1" width [29]. The DCB samples have a pre-crack built in and are pulled in tensile by the hinges. DCB allows for G_{IC} values to be calculated out.

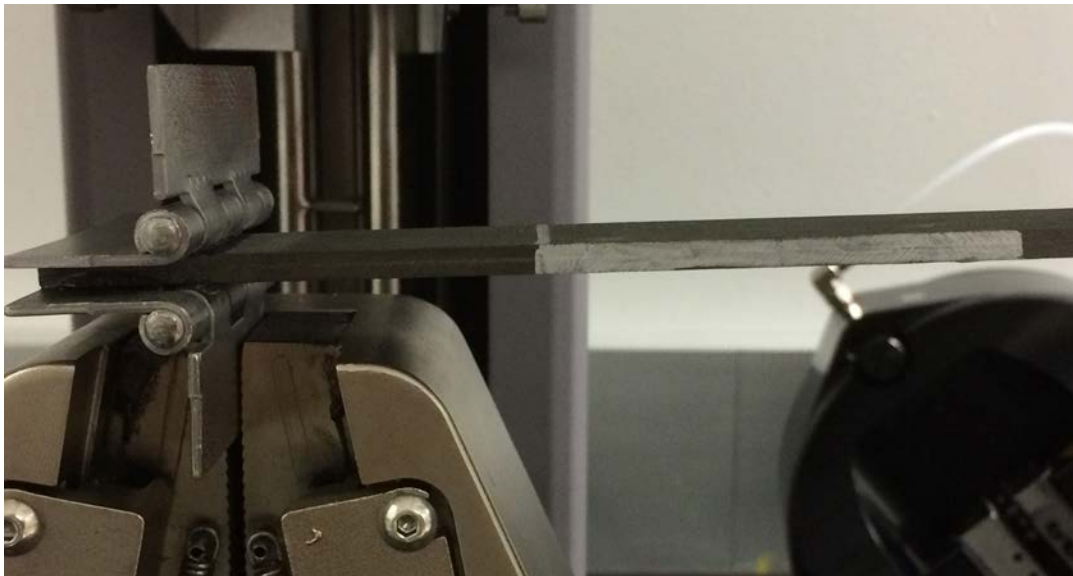


Figure 7. DCB Sample Setup

End-Notched Flexure (ENF) testing or also known as three point bending test is a form of mode II testing. Figure 8 shows the diagram of a typical ENF fixture. The fixture contains two parts, a base where there are two support rollers to place the ENF samples on and loading roller that is used to apply compression in the center of the sample.

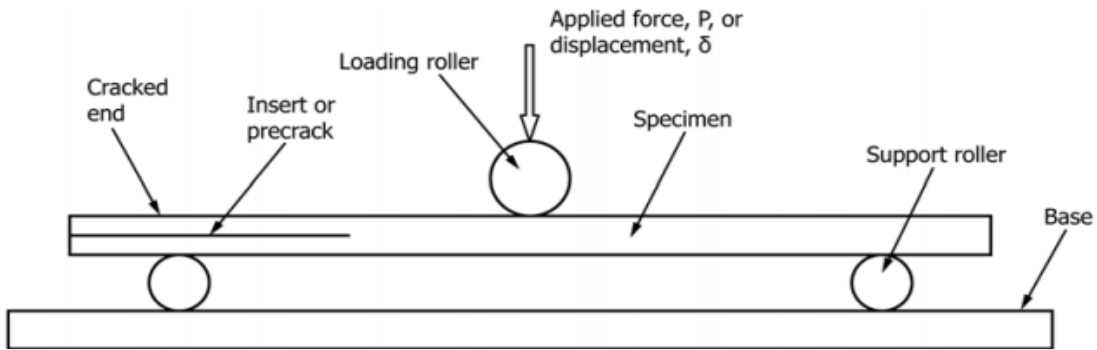


Figure 8. ENF Fixture and Sample Loading Diagram. Image obtained from ASTM Standard D7905/D7905M 2014

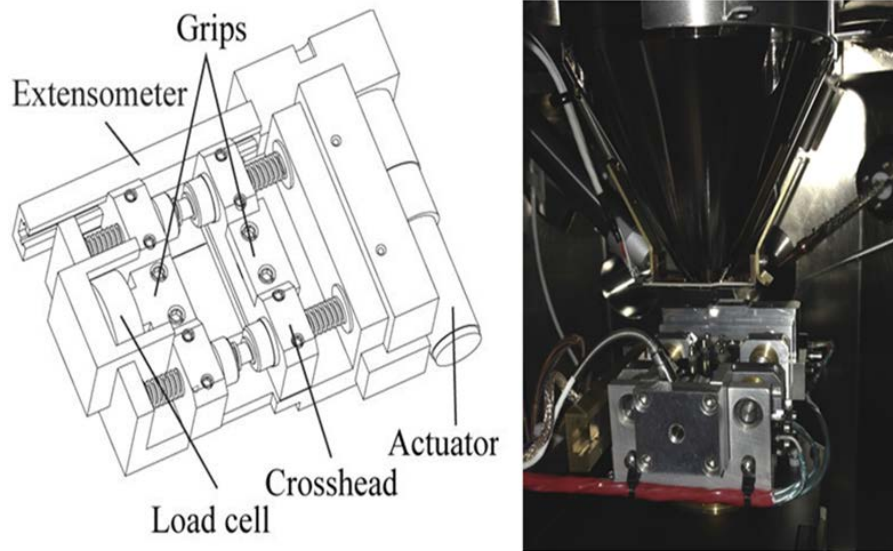


Figure 9. ENF Fixture for In-situ FIB-SEM

Using ASTM standards, ENF samples are manufactured with a pre-crack of known length with respect to remaining un-cracked length. Specific loading rates range from 0.10 mm/min to 0.80 mm/min with unloading rates ranging 0.10 mm/min to 1.6 mm/min [30]. Using fracture theory, the CERR in mode II can be calculated as $G_{IIc} =$

$$\frac{9F^{crit}\Delta_{ENF}^{crit}a_0^2}{2w(l^3/4+3a_0^3)} \cdot 1000 \text{ [27]}. F^{crit} \text{ refers to the critical load, } \Delta_{ENF}^{crit} \text{ refers to the loading}$$

displacement, w refers to width of the sample, l refers to the length of the un-cracked sample, and a_0 refers to the pre-crack length.

ENF testing can also be further exploited with in-situ testing via FIB-SEM.

Taking advantage of the imaging and real time video capture of crack propagation allows visual understanding on how fracture properties work on the micro-scale. With differences of size scales, redesigning of the test apparatus and specimen must be taken into account. Figure 9 shows an apparatus stage where it can be loaded into the chamber of the FIB-SEM. The camera of the FIB-SEM can then be focused to the sample that was loaded into the stage where the stage then applies compression to induce a mode II stress.

Mode III is not commonly used as it is the most complicated one of the three modes. The samples are loaded in shear mode however the shear stress applied is out of plane or perpendicular to the material length which is also known as a tearing motion (figure 6). Other modes that are also studied include a mixture of the previous mentioned modes. In this case, the applied stress has components of mode I and II [31]. Figure 10 shows a typical setup for mix mode sample testing. Mix mode will allow for calculations of G_C values however it is more complicated as determination of percentages of mode I and mode II of the test must be taken into account to calculate G_C values.

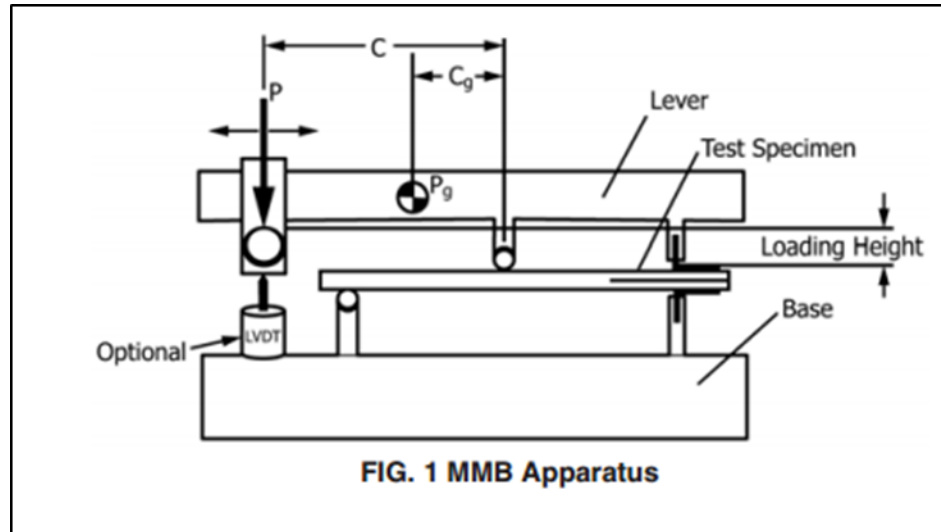


Figure 10. Mix Mode Sample Setup [31]

LAP-SHEAR TESTING

Lap-shear testing allows for quick and fast testing and analysis of the adhesive strength. This makes it a very common way to test adhesives. Lap-shear testing for CFRP has been standardized in accordance to ASTM D5868 – 01[32]. In lap-shear testing, the sample is pulled apart linearly until it breaks giving ultimate shear strength. Most testing is done with a tensile tester machine (figure 11). ASTM standards recommends for each lap-shear specimen to have a 1"x1" area bonded area with overall dimensions of 1"x7" (figure 12). For a reliable data set, sample sets of minimum 4-5 are preferred. When samples are broken via the MTS machine, the peak load and stress are given. Generally lap-shear test are simple to perform and quite common in testing adhesives. Lap-shear cannot be categorized as a mode of test as there is no pre-crack built in the samples.



Figure 11. MTS Criterion Model 43

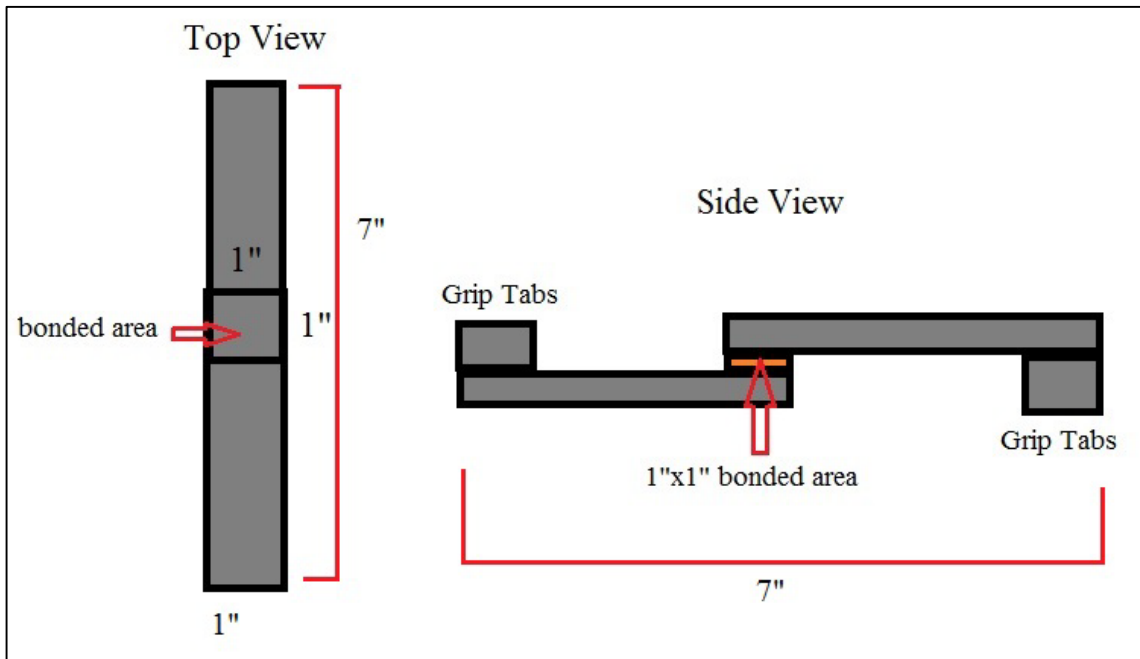


Figure 12. Lap-shear Sample Dimensions

CHAPTER III - METHODOLOGY

MATERIALS SELECTION

All carbon fiber panels manufactured were performed using pre-preg. Pre-preg carbon fiber material is a premade material that has carbon fibers laid out in one direction with epoxy resin to fill in as the matrix. The pre-preg comes in a roll which you can cut into sheets. When the sheets are cut, they then can be placed or “stacked” onto one another to manufacturer’s desired orientation. Due to the pre-preg being premade, it comes with a recommended preset of curing cycle and known mechanical properties.

Typical materials used in the fabrication process of the composite include vacuum bagging, breather material, peel ply, aluminum plates, vacuum tape, release ply and high temperature tape. When the layout process is complete, sheets of polyester peel ply is cut to the same dimensions of the laminate and layered on top of the laminate. A curing plate is used to hold the laminates which can be fitted into the autoclave to be cured.

Additional aluminum plates that are 24”x24” in dimensions are also placed on the laminates to help provide weighted pressure when curing. Breather material is also placed over the aluminum plates to help absorb excess epoxy resin during the curing cycle. Thermocouples are then placed into each side of the curing plate to monitor temperatures during curing cycle. Thermocouples and laminates are then vacuum sealed using vacuum sealant tape and high temperature tape.

After the laminates are cured they can be cut to specified dimensions and ready to be bonded. An epoxy two part based adhesive is used to bond two laminates together. The epoxy uses two parts base to one part hardener mixing component. After thorough mixing, the adhesive is then applied equally onto the designated bonding area of the

laminates. A small vacuum is applied to ensure equal pressure is applied until the adhesive fully cures. Similarly for doped experiments, a measured 1 volume percent was mixed into the base first then followed by addition and mixing of the hardener. A table is provided below for material model and manufacturer name.

Table 1. Materials used in Study

Pre-preg	Toray T800H
Peel Ply	Polyester Peel Ply (Fibre Glast)
Breather Material	Polyethylene Breather and Bleeder (Fibre Glast)
Release Ply	Low Temperature Release Film (Fibre Glast)
Vacuum Bag	Stretchlon 200 Bagging Film (Fibre Glast)
Vacuum Tape	Gray Sealant Tape (Fibre Glast)
High Temperature Tape	Flash Tape (Fibre Glast)
2 Part Epoxy Adhesive	3M Scotch-Weld Epoxy Adhesive EC-2615 B/A
MENs	Cobalt Ferrite-Barium Titanate (manufactured by Dr. Khizroev's group)
Spacers	Polycarbonate Sheet (0.4mm thickness) - ENF Aluminum Sheet (0.3mm thickness) – Lap-shear

DISPERSION OF MENS

The type of MENs used was cobalt ferrite-barium titanate ($\text{CoFe}_2\text{O}_4\text{-BaTiO}_3$). Typically with high viscous liquids, sonication is not recommended. Due to the high viscosity the vibrational energy provided by the sonication machine is not sufficient to allow proper mixing. Other methods involve the use of metallic balls where they are used to rotate and mix in the components. Ball mixing is a viable option however due to the small volume use it is extremely difficult. Attributing to the same problem, the use of a small volume of adhesive was not easy to incorporate conventional mixing methods. Due to the given conditions, hand mixing was the best option for dispersing MENs into the

adhesive. MENs were measured based on the total volume of the adhesive at 1 volume percent. Once measured, the MENs are first mixed with the base slowly in a circular motion. With thorough mixing, the hardener is then mixed into the base with MENs.

ASSESSMENT OF DISPERSION

Currently there are techniques that can be performed to assess the dispersion of MENs. One technique that can be used is a process called TEM lift-out. A thin sheet of the sample is cutout. The thin sheet then is extracted onto a TEM grid and placed in the TEM for characterization. Characterization allows us to identify localized dispersion of the MENs and their atomic lattice spacing by calculating out the distance between planes (d-spacing). Figure 13 shows the d-spacing calculations with distance of 2.1 angstroms. The measurements match well with The International Center for Diffraction Data Powder Diffraction File (ICCD PDF) value of 2.0999 angstroms.

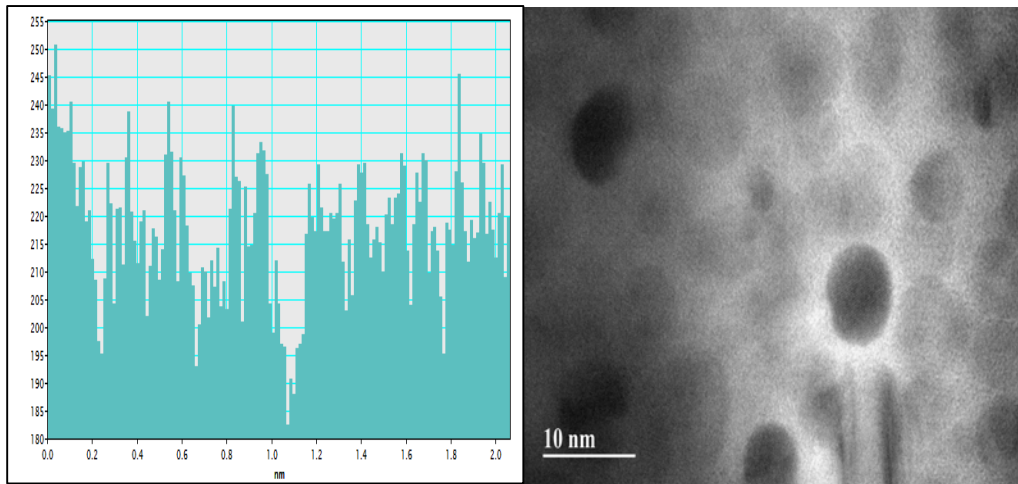


Figure 13. D-spacing for CoFe_2O_4 with 2.1 Angstroms

BOND LINE MEASURING

As mentioned in the literature review, bond line thickness must be considered when accessing properties such as fracture toughness. There is an optimum bond line

thickness that allows for maximization of fracture energy. When the bond line thickness becomes too thick, the fracture energy values become more like the bulk material and thus losing out of the combined property of adhesive and composite. When the bond line thickness falls below of the optimum thickness, it also decreases the fracture energy. This is due to the fact that thinner bond lines are much more likely to fail adhesively which requires less energy than cohesive failures.

All ENF and lap-shear samples were measured for bond line thickness before mechanical testing. An optical microscope was used to image the bond line with the ZEN program by Zeiss Company to measure the thickness. Bond line measurements were measured three times on each side of the sample to obtain good data set for averaging. One side of the sample was first measured and labeled as the left or right side. Then that selected side is divided into three sections: left, center and right. The same procedure was then performed for the remaining side. With the measurements made, averages of each side can be tabulated and a total average of the sample can then be calculated out. Figure 14 below shows an image that shows a bond line thickness measurement for reference. Bond line measurements are very important to measure and record as bonding strength is affected by the bond line thickness. In analysis it is important to relate the specific strength of certain samples to their bond line to determine outliers.

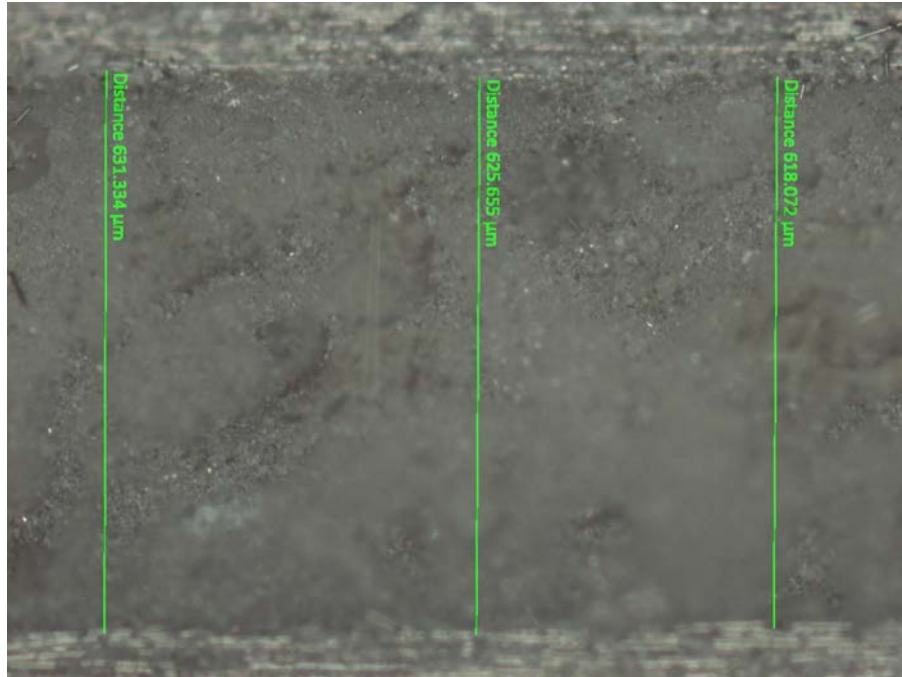


Figure 14. Bond Line Measurement of Lap-Shear Sample

LAP-SHEAR MANUFACTURING AND TESTING

The pre-preg sheets were stacked in a unidirectional setup with total of 12 layers. After curing, lap-shear laminate was cut with a table saw in half with each half having dimensions of 11"x10". The two halves were then trimmed by cutting off tabs with dimensions of 1"x11". The tabs then are super glued onto the ends of the laminates in the longitudinal side. The two halves are then stacked on top of each other to have a 1"x11" bonded area. In attempt to control the bond line to ASTM standards nominal thickness of 0.0762 mm, aluminum sheets with 0.6mm thickness spacers were used. The individual samples then can be cut out from the bonded laminates. Lap-shear samples were cut to have a total dimension of 1" x7" with a total of 1"x1" bonded area in each sample. Single lap-shear samples followed testing methods described in ASTM D5868-01. The samples were tested with the MTS Criterion Model 43. The loading rate was set to 0.5"/minute

with four samples of un-doped and doped samples. Lap-shear samples are loaded in mechanical grippers as opposed to the pneumatic grippers as they apply too much pressure and could damage the tabs. The samples are configured in the vertical direction as seen in figure 15. Peak load and peak stress was recorded in the test.



Figure 15. Lap-shear Sample Configuration for MTS Criterion Model 43

ASSESSMENT OF LAP-SHEAR TESTING

Lap-shear samples do not have a pre-crack as the entire bonding area is completely bonded thus G_I/G_{II} values cannot be obtained. When the lap-shear samples are loaded into the testing machine and broken, the software records the displacement of the crosshead and specific load. This information is then displayed into a load vs. displacement graph. When the sample breaks, that specific load to that fracture point is then recorded as the peak stress and peak strain.

ENF MANUFACTURING AND TESTING

All micro-scale testing will be performed using ENF testing. ENF testing will be performed outside and in-situ via SEM-FIB using a MTI Instrument SEM 1000 Tester as the test apparatus. All test runs will be performed in real time to record displacement and load values. All ENF samples were manufactured with 10 sheets all orientated at 0°. Two polycarbonate spacers with total thickness of 0.8mm was cutout with two square holes of 50mmx50mm (figure 16) was cut out with sides approximately 5mm bezels surrounding the square holes. One of the spacers is placed on top on the laminate. The adhesive is then spread and applied to the cut out squares to fill in the square holes. A single rectangular sheet of release ply is then cut out and placed directly covering the first 14mm of the cutout squares to create the pre-crack. The second cut out spacer is then aligned on top of the placed spacer sandwiching the release ply. The bonded laminates are then put under vacuum for 24 hours.

In order for the samples to be observed and fitted to the test apparatus, samples dimensions were cut to 10mmx35mm size with 14mm pre-crack. The edges of the laminate would be cut out to remove the spacer followed by cutting the remaining laminate to specified dimensions. To minimize the edge effects, ENF samples were cut with the water jet. Water jet is much better at minimizing edge effects due to the high amount of water pressure (15,000-50,000 PSI) supplied through a small nozzle compared to a standard thick saw blade. The jet stream is accurately controlled through the use of a computer numerical controlled (CNC) tool which allows high precision over the conventional methods. The samples were then placed in the micro-stage for testing with loading rates of 0.5mm/minute as per ASTM D7905.

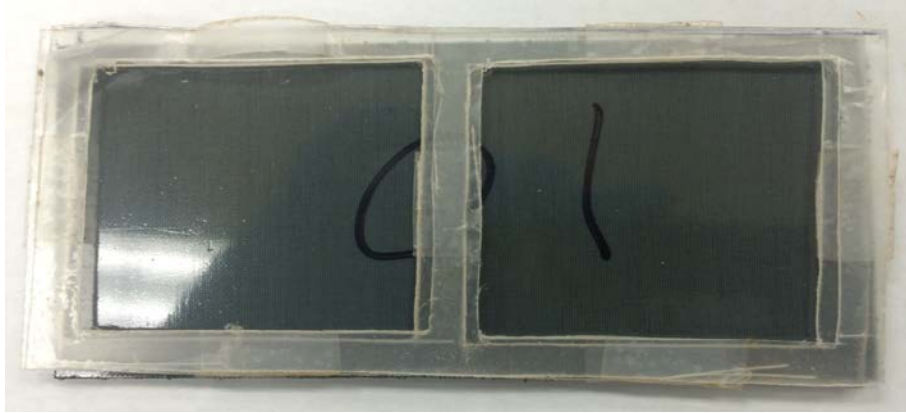


Figure 16. Spacer Cutouts to be placed on Top of the Laminate

ASSESSMENT OF ENF TESTING

G_{II} values of the samples were obtained instead as opposed to G_{IIC} values. Due to the configuration and nature of the small ENF samples, it is hard to determine the correct critical load at which the crack to propagates. Instead, the samples were all subjected to a maximum fracture displacement with the corresponding force. G_{II} values were calculated from the following equation: $G_{II} = \frac{9a^2 P \delta}{2\beta(2l^3 + 3a^3)}$. In the equation, “a” is the pre-crack, “P” is the load, “ δ ” is the displacement of the pre-crack, “ β ” is the width of the ENF samples and “l” is the distance between the two bottom points from the three point bend test fixture which is fixed at 16.5mm. This equation gives the units of the G_{II} values in kJ/m^2 . In addition, load vs. displacement graphs can be plotted out from the raw data for comparisons between the samples.

ADHESIVE SCANNING

Initial testing of magnetic measurements on cured adhesives was performed. Two sets of adhesive samples were cured, un-doped and doped samples. A reverse mold was

3D printed with 9 reverse cutouts with dimensions of 5mmx5mmx1mm. A two part silicone polymer was mixed and added to the reverse mold to create the actual mold. After the mold has cured, the adhesive samples of un-doped and doped adhesive will be mixed and placed into the 9 cutouts in the mold. The adhesive samples were cured for 24 hours. After fully curing, the samples were cut and sanded to remove uneven surfaces and send for scanning. Additional doped samples were then placed in an environmental chamber at 70°C and 95% relative humidity.

Adhesives samples were scanned with the vibrating sample magnetometer (VSM). The sample is placed inside a magnetic field with pickup coils on both sides of the magnet. A sinusoidal wave is then applied giving the magnetization and magnetic field measurements. Doped samples will give a hysteresis loop due to the relaxation of the magnetization being nonzero from the MENs. Comparisons of environmentally exposed and baseline doped will help ensure that the MENs can serve as the multifunctional effect

CHAPTER IV – RESULTS

BOND LINE MEASUREMENTS

Tables 2 and 3 below represent the average bond line measurements for each side along with the total averages in a quantitative view. For the lap-shear samples, the bond line thickness values did fall within the 3M recommendations with the exception of sample 1 (see figures 17 and 18) [33]. The slight inconsistency with the left and right bond line is attributed to the inward bowing of the lap-shear bonded laminates during the curing process. The bowing process allowed the edge sided samples that were cut to have a thicker bond line. The bowing effect was caused due to the nature of the spacer placement with the applied vacuum. The intention for future manufacturing and process is to use the polycarbonate spacers used for the ENF samples as it produces a more reliable and consistent bond line thickness.

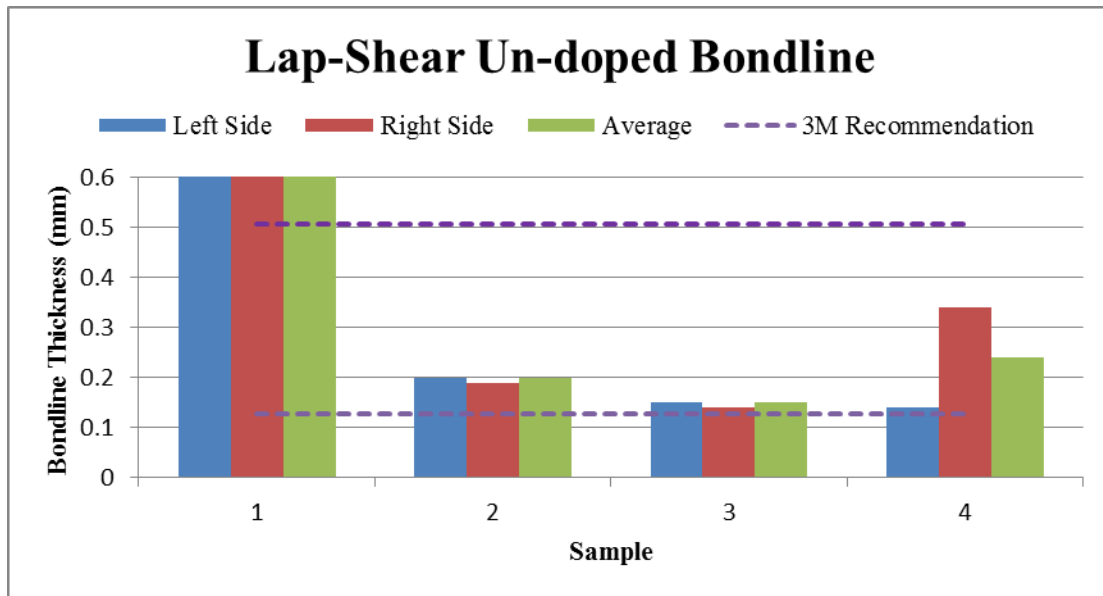


Figure 17. Bond Line Measurements of Lap-Shear Un-doped

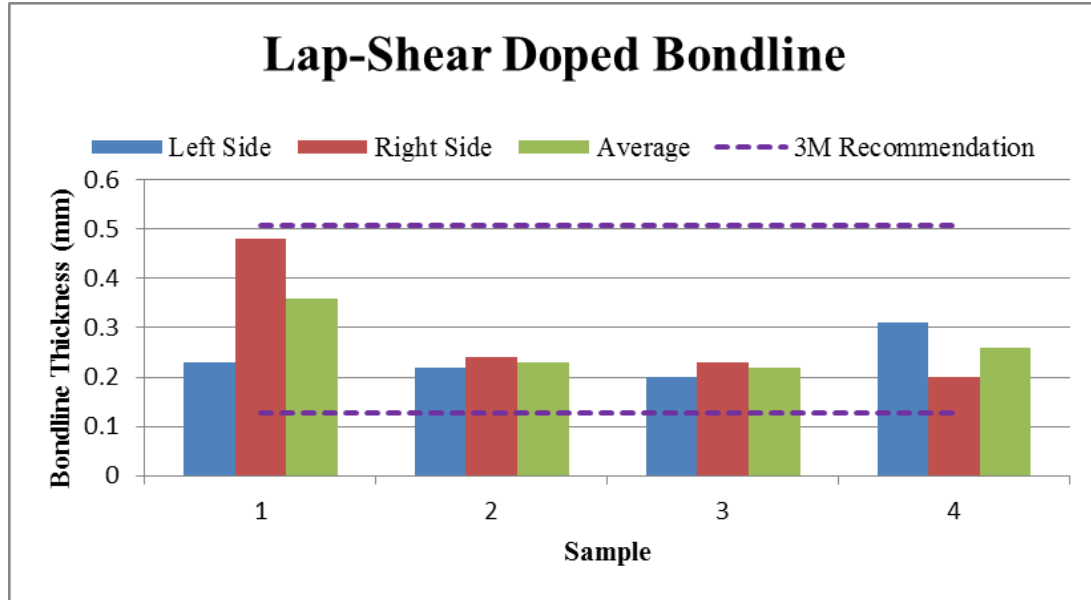


Figure 18. Bond Line Measurements of Lap-Shear Doped

Table 2. Average Bond Line Measurements of Un-doped Lap-Shear

	Left Side Average (mm)	Right Side Average (mm)	Total Average (mm)
Sample 1	0.61	0.61	0.61
Sample 2	0.20	0.19	0.20
Sample 3	0.15	0.14	0.15
Sample 4	0.14	0.34	0.24

Table 3. Average Bond Line Measurements of Doped 1 vol. % Lap-Shear

	Left Side Average (mm)	Right Side Average (mm)	Total Average (mm)
Sample 1	0.23	0.48	0.36
Sample 2	0.22	0.24	0.23
Sample 3	0.20	0.23	0.22
Sample 4	0.31	0.20	0.26
Sample 5	0.58	0.16	0.37
Sample 6	0.14	0.58	0.36

In the ENF bond line measurements, the measurements were consistent throughout the left side/right side and each sample. The average bond line thickness for

the un-doped ENF samples are 1.14 mm and for doped samples are 1.27 mm. The spacer was designed to keep the bond line within 800 μ m however the increased in thickness can be attributed to the expansion of the adhesive during cross-linking process. Figures 19 and 20 displays the graphs of the bond line measurements with averages. Due to the fact the ENF standards [30] does not require a specific bond line thickness, the consistency of the bond line thickness was the primary concern. Table 4 and 5 are also provided below for a quantitative view.

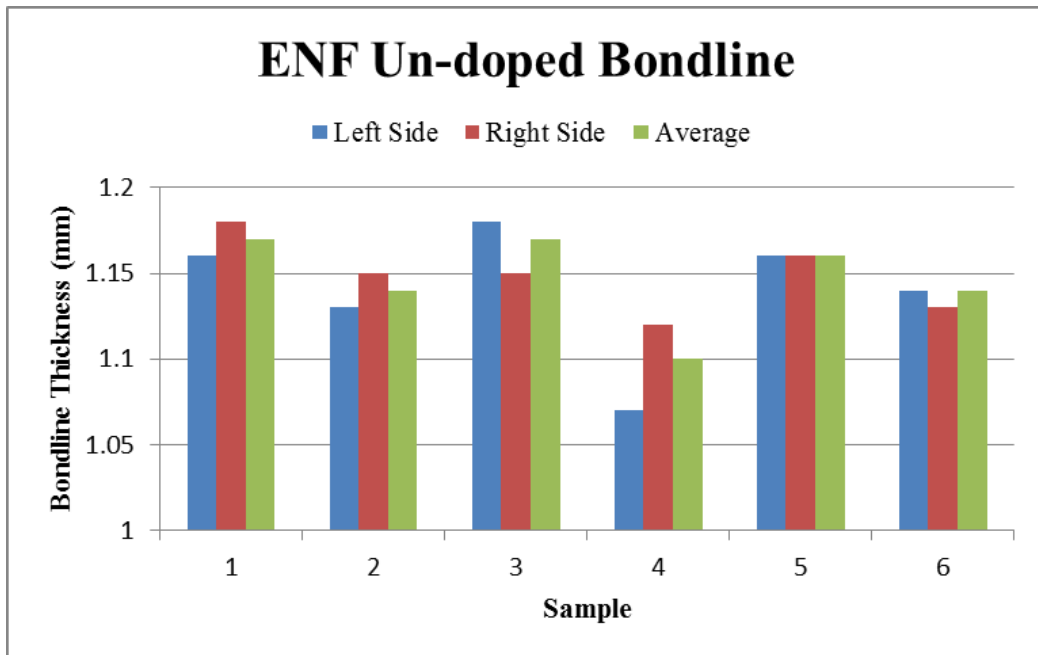


Figure 19. Bond Line Measurements of ENF Un-doped

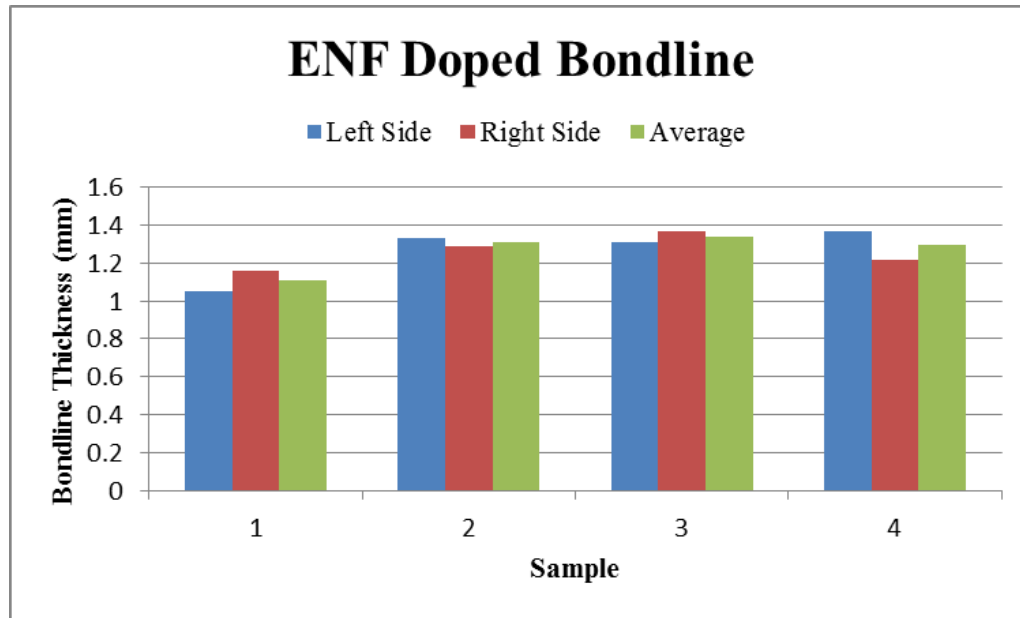


Figure 20. Bond Line Measurement of ENF Doped

Table 4. Average Bond Line Measurements of Un-doped ENF Samples

	Left Side Average (mm)	Right Side Average (mm)	Total Average (mm)
Sample 1	1.16	1.18	1.17
Sample 2	1.13	1.15	1.14
Sample 3	1.13	1.15	1.14
Sample 4	1.07	1.12	1.10

Table 5. Average Bond Line Measurements of Doped 1 vol. % ENF Samples

	Left Side Average (mm)	Right Side Average (mm)	Total Average (mm)
Sample 1	1.05	1.16	1.11
Sample 2	1.33	1.29	1.31
Sample 3	1.31	1.37	1.34
Sample 4	1.37	1.22	1.30

UN-DOPED LAP-SHEAR RESULTS

The average peak load for un-doped lap-shear samples was 16.14 kN with an average peak stress of 25 Mpa. Table 6 gives the peak load/stress values along with the

averages. Figure 21 shows the load vs. displacement curves of the samples. It is seen here that the samples follow the same loading path with nearly identical slopes. Sample 2 had a lower peak load rate however the bond line thickness still fell within the recommendations.

Table 6. Un-doped Lap-Shear Peak Load/Stress

	Peak Load (kN)	Peak Stress (Mpa)
Sample 1	17.46	27
Sample 2	14.04	22
Sample 3	15.64	24
Sample 4	17.42	27
Average (mean)	16.14	25
Standard Deviation	1.64	2.45

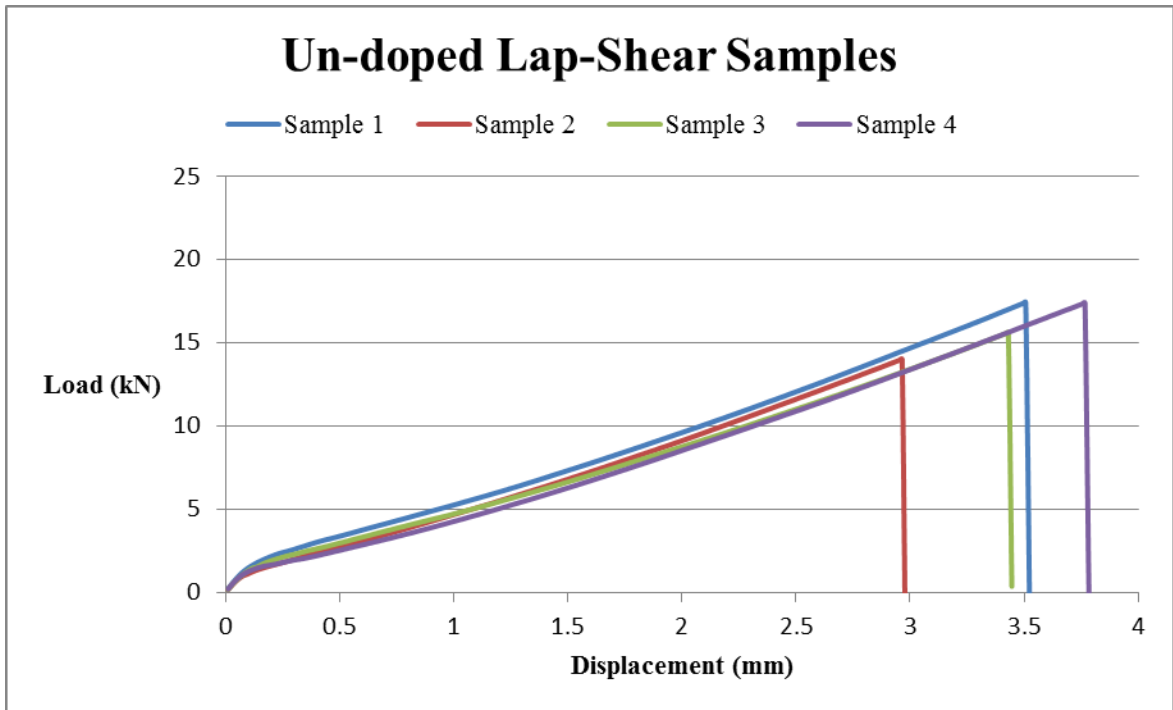


Figure 21. Load Displacement Graphs of Un-doped Lap-Shear

DOPED LAP-SHEAR RESULTS

The doped samples at 1 vol. % had an average peak load of 19.87 kN with an average peak stress of 31 Mpa. Doped samples here have very similar loading graphs

with nearly identical slopes. Table 7 below shows the obtained peak load and stress values from testing along with figure 22 displaying the load vs. displacement graphs.

Table 7. Doped Samples 1 vol. % Peak Load/Stress

	Peak Load (kN)	Peak Stress (Mpa)
Sample 1	17.79	28
Sample 2	20.09	31
Sample 3	21.25	33
Sample 4	20.33	32
Average (mean)	19.87	31
Standard Deviation	1.47	2.16

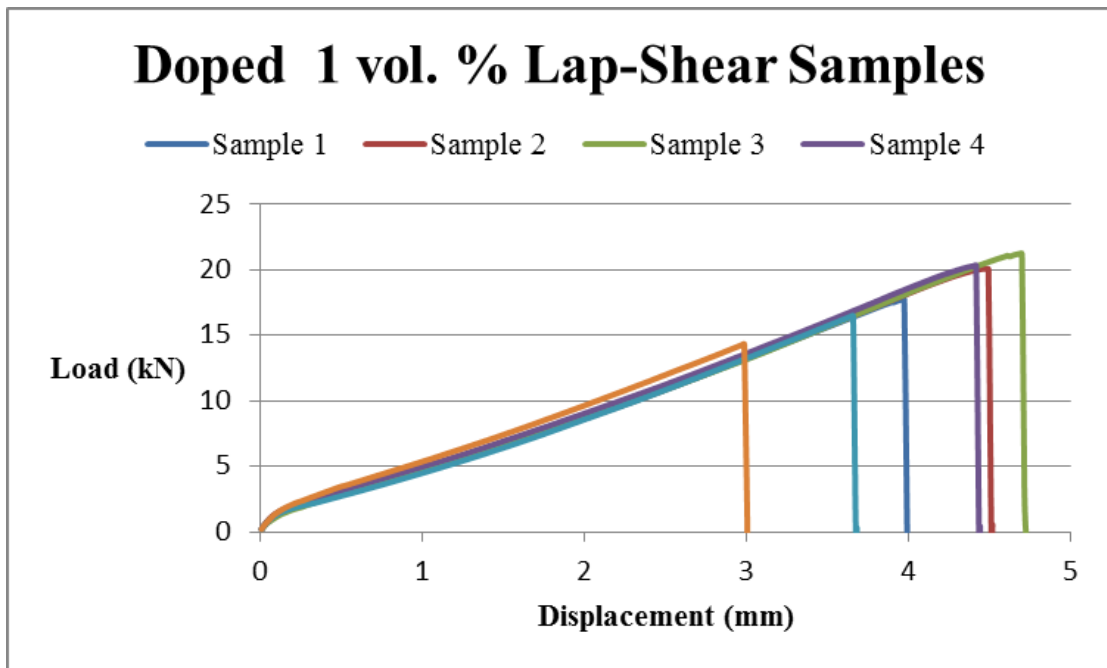


Figure 22. Load vs. Displacement Graph of Doped 1 vol. % Lap-Shear

UN-DOPED AND DOPED LAP-SHEAR COMPARISON

By comparison, the doped samples had an average of 19.87 kN for peak load over un-doped's 16.14 kN or about 23% increase in strength. Similarly the peak stress has also improved over the un-doped samples by about 13%. A doping concentration of 1 vol. %

has improved the bonding strength of the lap-shear samples overall. In figures 23 and 24, the graph shows the averages of the peak load and stress of the samples in comparison.

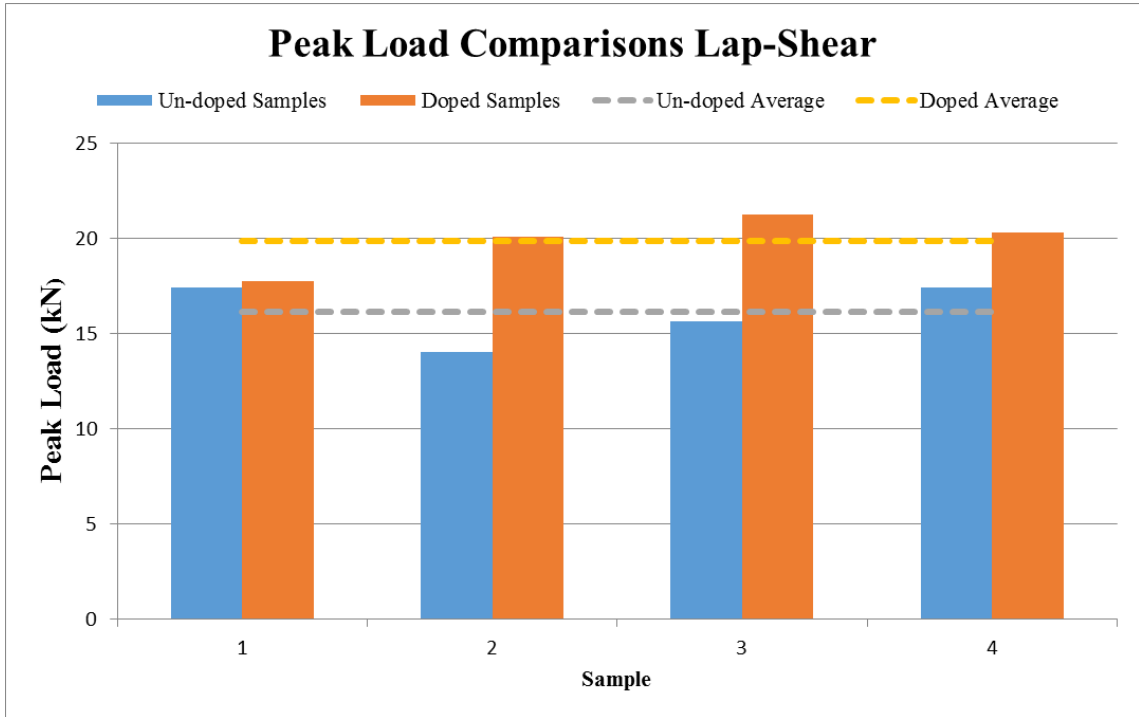


Figure 23. Averages of the Peak Load for Lap-Shear Comparisons

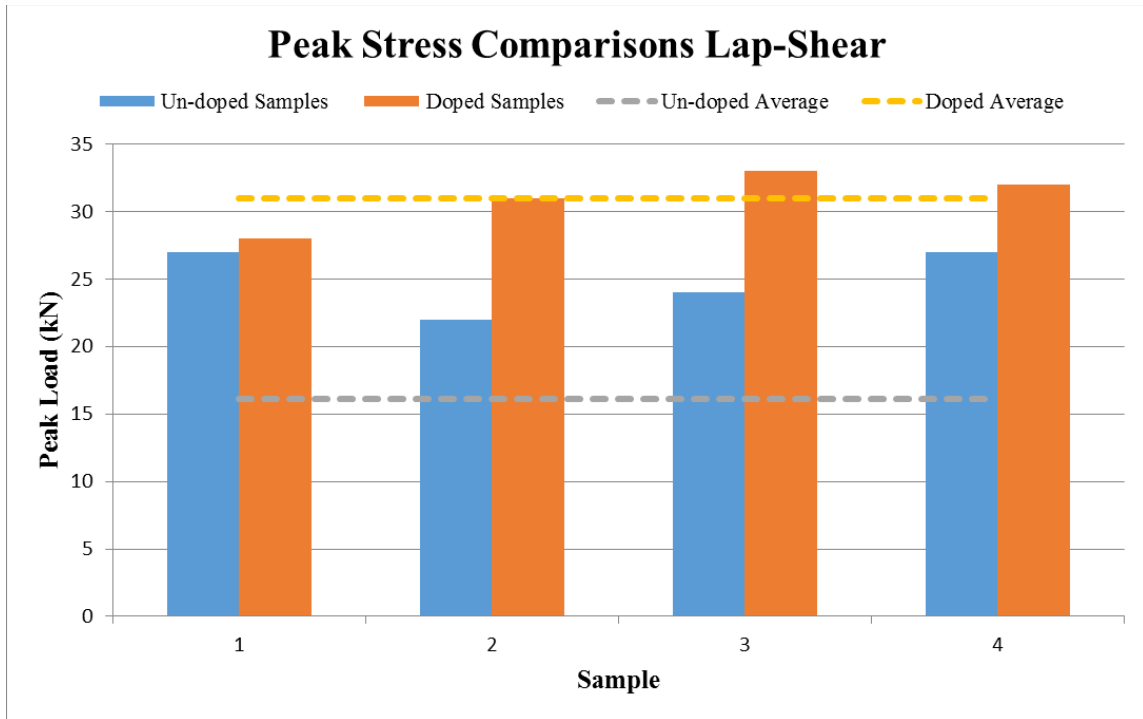


Figure 24. Averages of the Peak Stress for Lap-Shear Comparisons

UN-DOPED ENF G_{II} RESULTS

All ENF samples were placed under microscope to have their pre-crack measured. The pre-crack is measured beforehand as it is integral in calculating out the G_{II} values. In the same way other dimensions were measured out such as the width, length and thickness. Table 8 shows the values of the samples with the averages. Under load, the pre-crack was loaded to a known load value at 2750 N with corresponding displacement thus giving G_{II} values.

Table 8. Dimensions and Crack Measurements of ENF Un-doped Samples

Sample	Width - B (mm)	Length - l (mm)	Thickness -2h (mm)	Pre-crack - a (mm)
1	10.31	35.09	4.57	13.86
2	10.33	35.14	4.6	14.09
3	10.28	35.11	4.61	13.65
4	10.31	35.12	4.62	14.12
Average	10.32	35.11	4.60	13.93
Standard Deviation	0.03	0.02	0.02	0.22

Table 9 reports the G_{II} , Load and displacement values of the samples tested.

Figure 25 shows the load displacement curves for the tested specimens. The load displacement curves are very consistent within the elastic regime. The initial portion of the load displacement curves is due to the system settling and balances out as the curves become more linear. Since G_{II} values were reported, it is important to note that the lower G_{II} values correspond to better material. G_{II} is the amount of energy that is held at the specific displacement and not the amount of energy released.

Table 9. G_{II} Values of Un-doped samples with Load/Displacement

Sample	G_{II} (kJ/m ²)	Load (N)	Displacement (mm)
1	20.43	2750.02	1.50
2	21.16	2750.01	1.55
3	17.10	2750.01	1.27
4	15.61	2750.02	1.14
Average	18.57	2750.01	1.36
Standard Deviation	2.65	0.0053	0.19

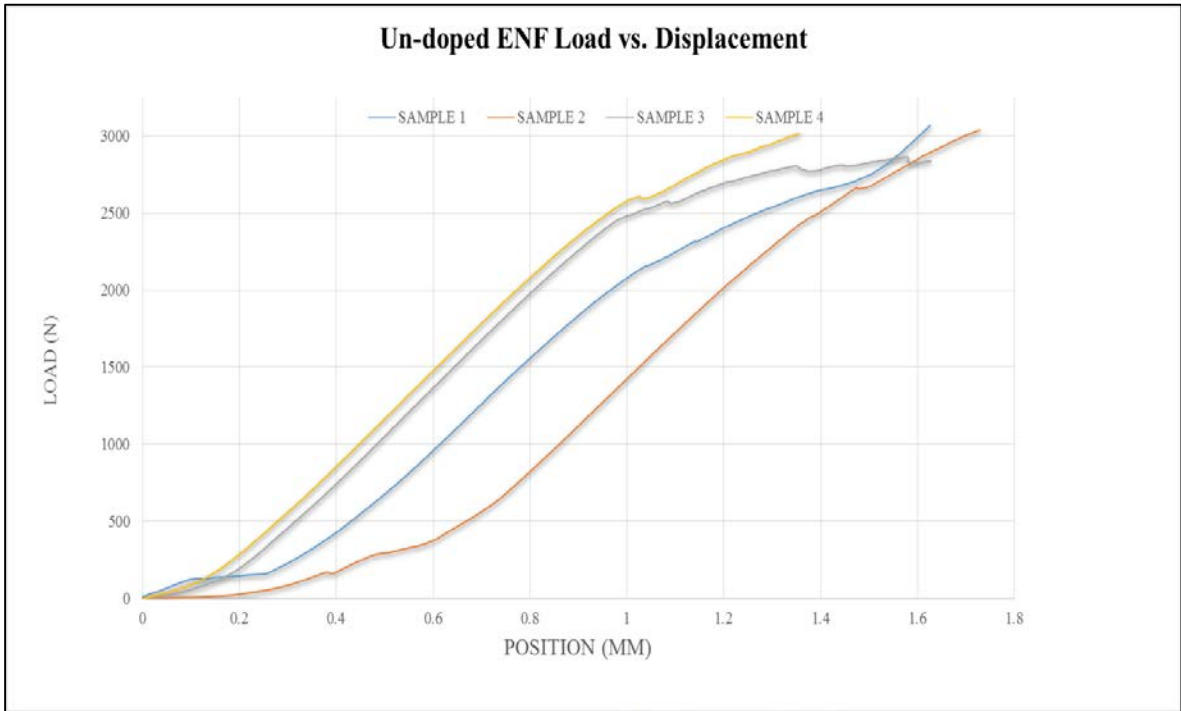


Figure 25. Load Displacement Graphs of Un-doped ENF Samples

DOPED ENF G_{II} RESULTS

All doped samples were subjected to same measurements and loading configurations. Table 10 gives the specific dimension of the doped samples with table 11 giving the specific G_{II} calculations with the corresponding load and displacement. The load displacement graph also shows very consistent elastic regime among the samples (figure 26).

Table 10. Dimensions and Crack Measurements of ENF Doped Samples

Sample	Width - B (mm)	Length - l (mm)	Thickness -2h (mm)	Pre-crack - a (mm)
1	10.10	34.92	4.56	0.67
2	10.10	34.94	4.77	0.60
3	10.09	34.97	4.66	0.60
4	10.08	34.95	4.63	0.60
Average	10.09	34.95	4.66	0.62
Standard Deviation	0.01	0.02	0.09	0.03

Table 11. G_{II} Values of Doped samples with Load/Displacement

Sample	G_{II} (kJ/m ²)	Load (N)	Displacement (mm)
1	5.96	2749.87	1.07
2	4.55	2750.02	0.99
3	5.33	2749.99	1.16
4	5.78	2750.02	1.25
Average	5.22	4749.97	1.12
Standard Deviation	0.62	0.07	0.11

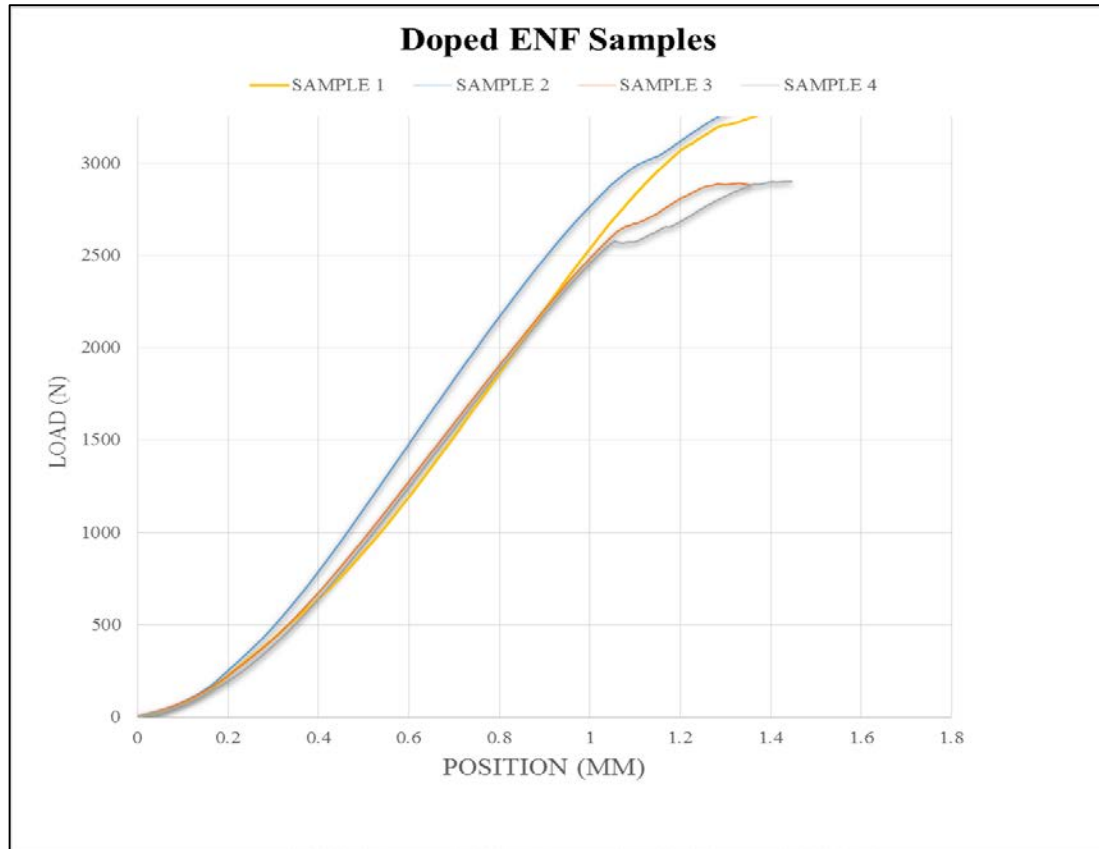


Figure 26. Load Displacement Graph of Doped ENF Samples

UN-DOPED AND DOPED ENF COMPARISON

The comparison of un-doped and doped ENF has shown improvements of the ability to experience less critical energy release rates at the same loading. The average G_{II} improvement of the doped ENF to un-doped was 3.6 times lower energy release rate at the crack tip. Higher values mean that the energy built up at the tip is closer to G_{IIC} or closer to failure. This result seen here is due to the “crack shielding” that the MENs provide; that is less energy focusing on the crack tip. Another component of the MENs is at the crack tip; propagation of the crack requires more energy due to the physical properties, such as hardness is higher than the adhesive. The slopes of the un-doped and

doped ENF was also compared (figure 27). It is seen here that the average slope of the doped ENF is higher than the un-doped ENF. The slope represents the samples stiffness or the amount of force required to displace the sample by 1 mm. The doped ENF had an average improvement of 264 N/mm over the un-doped.

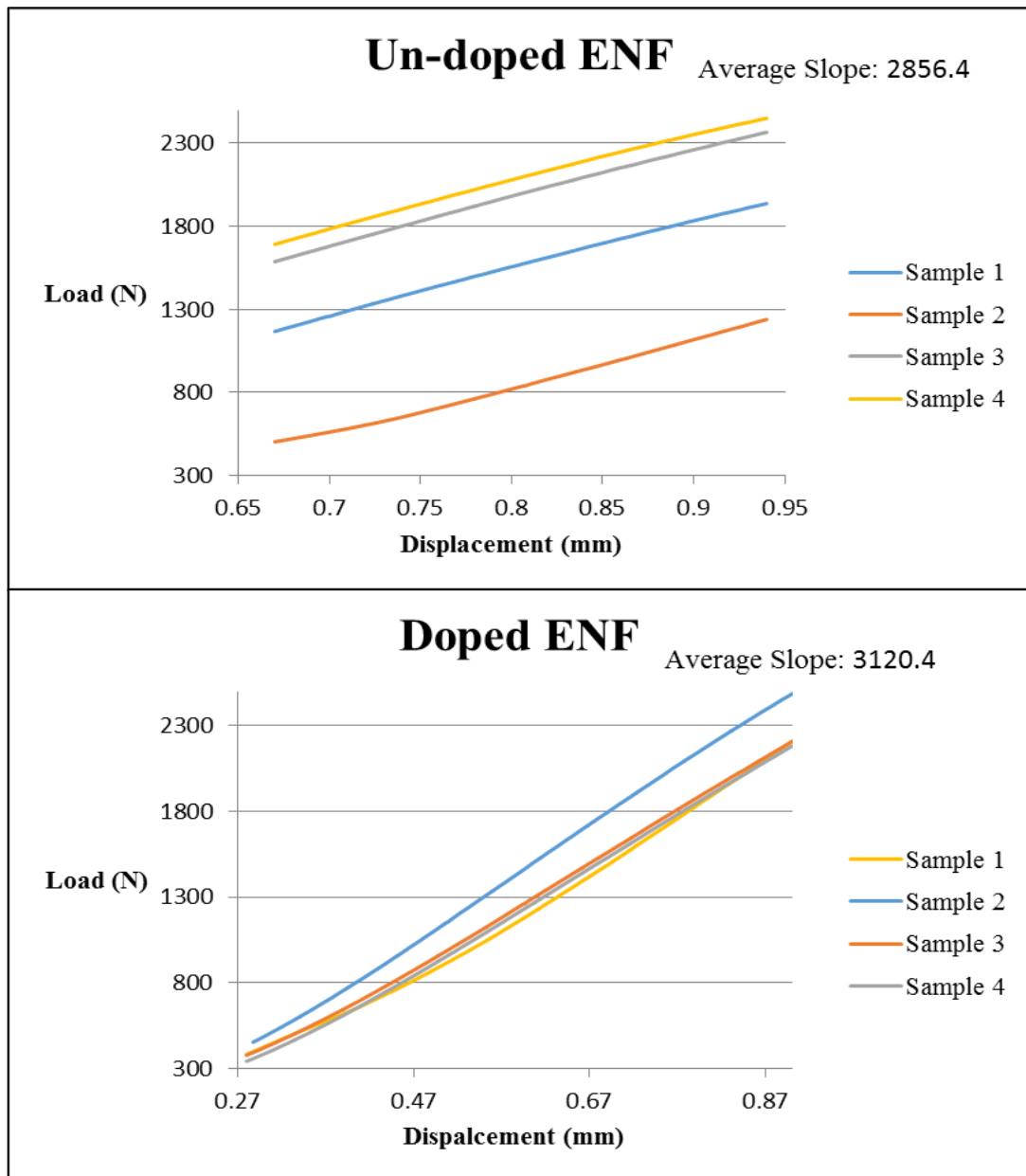


Figure 27. Un-doped and Doped ENF Comparisons

IN-SITU ENF RESULTS

Un-doped and doped samples were placed in the FIB-SEM chamber and observed for failure mechanisms. It is seen here that before loading, both un-doped and doped samples had large angles, however after loading the angles of the crack tip decreased. The loading of the crack tip has allowed the crack angle to change signifying there was damage that has occurred. The un-doped samples had a starting angle of about 89° and after loading it decreased to about 45° (figure 28). The doped samples started off with an angle of about 80° and after loading decreased to about 35° . It is also seen here that crack initiations were also observed above the crack tip at the highlighted regions (figure 29).

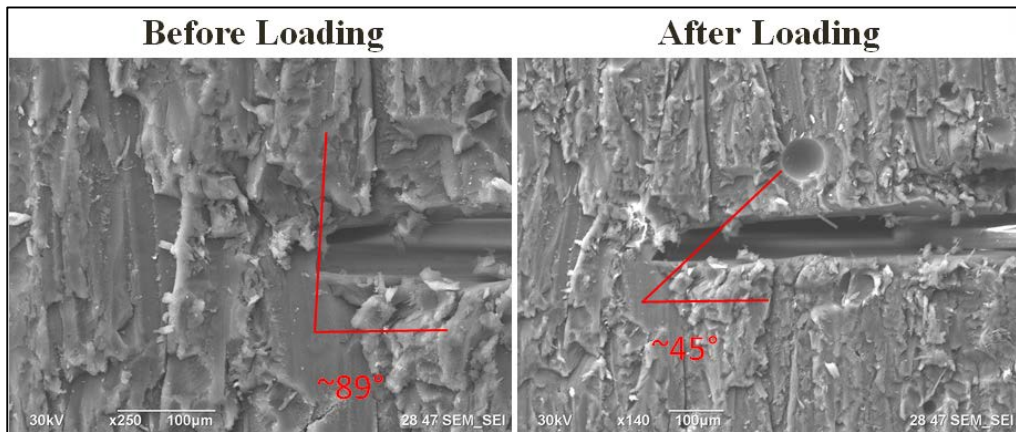


Figure 28. Un-doped Before and After Loading In-Situ

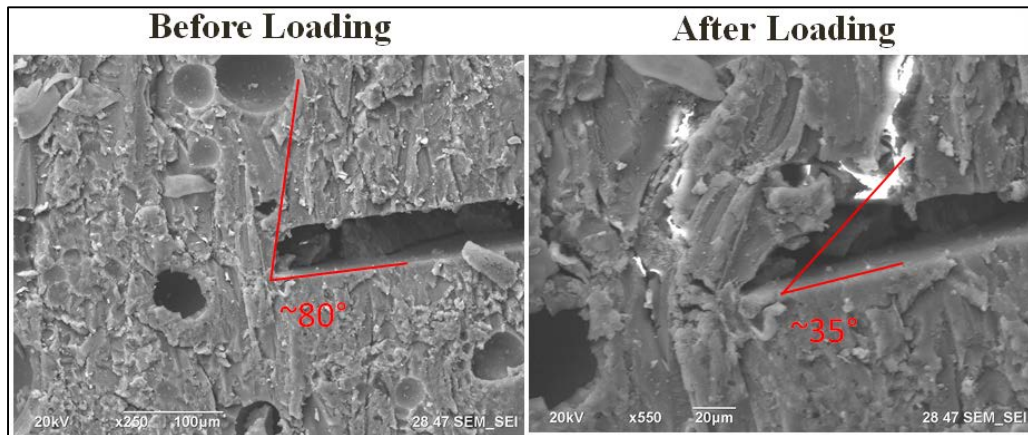


Figure 29. Doped Before and After Loading In-Situ

VIBRATING SCANNING MAGNETOMETRY RESULTS

The magnetic signatures of the adhesive samples were collected using a VSM. The first results provided are magnetic signatures of the epoxy-based adhesive samples doped with the 30nm MENs and the un-doped adhesive samples. These results can be seen in Figure 30. It can easily be observed that there is an order of magnitude difference between the magnetic signatures of the doped and un-doped baseline. These results verify the presence of MENs within the adhesive the shape of the hysteresis loop of the doped adhesive specimens is a “butterfly” shape which is characteristic of an antiparallel, or ferromagnetic, coupling of the magnetic spins.

Results below are magnetic signatures of the doped adhesive samples after a four week exposure period to the environmental chamber as seen in figure 31. It can be seen here that comparing the doped baseline to environmental exposed doped has magnitudes of order different in signals too. The difference in signal is attributed to the change in surface charge density of the MENs from the exposure. The exposure along with time, has allowed the chemistry of the adhesive/MENs to change thus changing the signal.

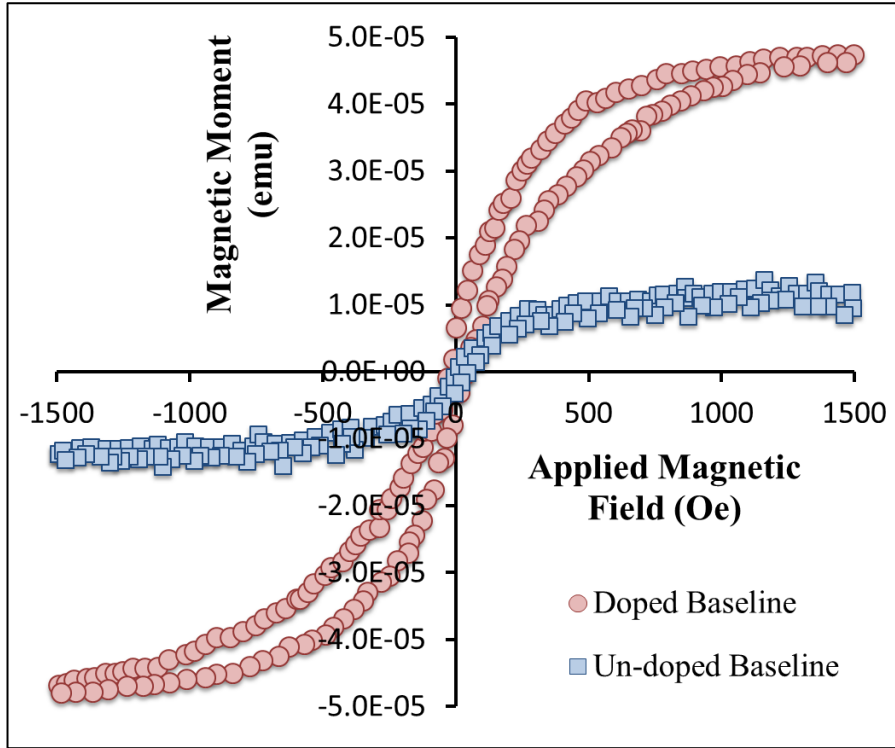


Figure 30. Magnetic Signatures of Un-doped and Doped Baselines

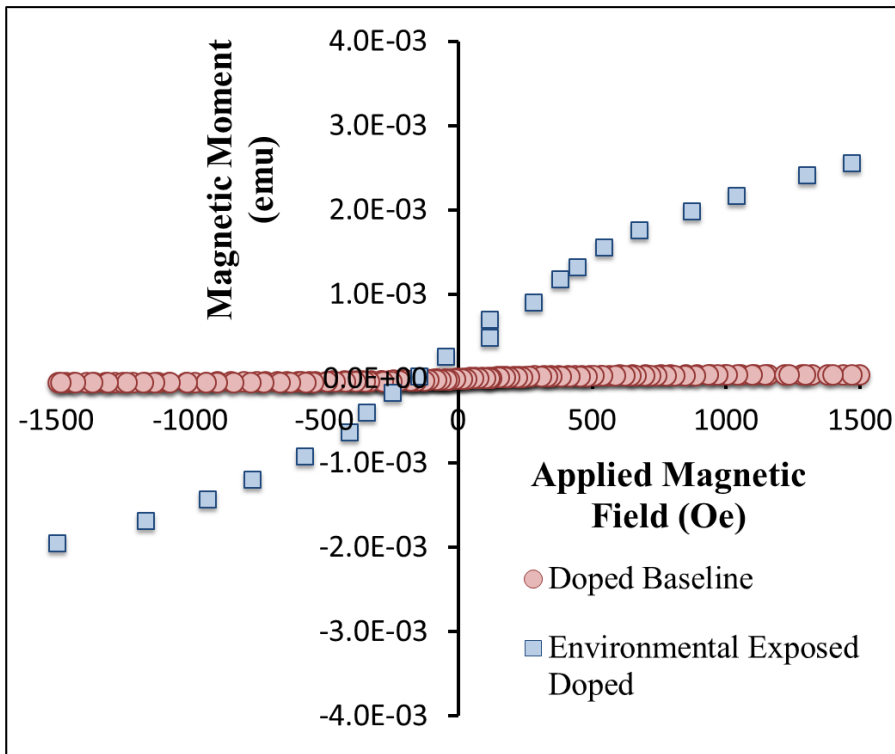
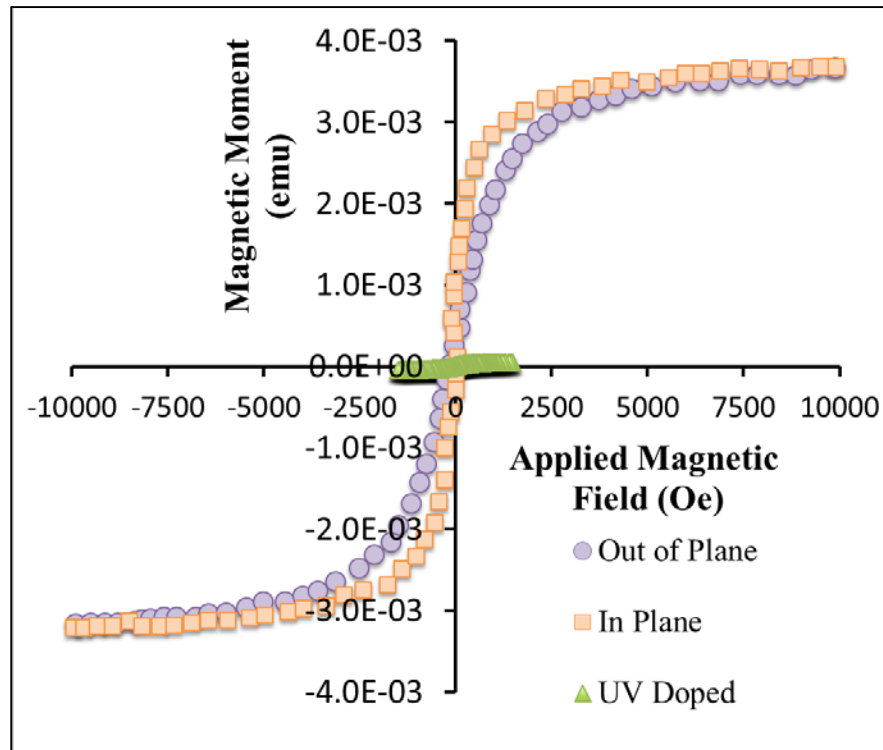


Figure 31. Magnetic Signature of Doped Baseline and Environmental Exposed Doped

Both in-plane and out-of-plane results are also provided in figure 32. When the magnetic field is aligned with the magnetic dipole of the MENs the scan is “In Plane”. When the field is not aligned, it is then called “Out of Plane”. It is seen here that in this situation, similar results are obtained for In Plane/Out of Plane environmental exposed doped samples. In addition, a UV exposed doped sample was also scanned. The 1 month exposure of UV radiation was shown to have no results as the scans are within noise levels. The results of all the magnetic signatures here are preliminary and help provide the baseline and continuation of the project.

Figure 32. Magnetic Signatures of Out of Plane/In Plane E.E. Doped and UV



CHAPTER V - DISCUSSION

RESEARCH CHALLENGES

An early challenge that was presented in the research was the dispersion of MENs and bond line control. Due to the selection of the adhesive, the viscosity was high and could not be mixed easily with the MENs. Another issue was the sheer volume of usage as it was not enough to use dispersive techniques such as ball milling. With all the restrictions and nature of our selection, hand mixing was the best method at our disposal. The hand mixing proved to work however; control of hand coordination and consistent mixing was difficult. This leads into the problem of assessing the distribution of MENs. However this problem is not only common in our project but a common problem in the particle disbursement community and needs to be addressed.

Bond line control in lap-shear samples proved to be an issue with first initial manufacturing runs. The vacuum pull does allow for even applied pressure however if the spacers are placed in a specific manner, flexing can occur. This issue was addressed in using spacers carefully cut out on each side of the lap-shear samples. This method minimizes the flex as the distance of the spacers are short leaving only areas with no spacers being the bonded area. Spacers used for the ENF has also been effective however when bonding doped adhesive, proper care must be taken care off to ensure there is enough pressure applied to minimize the amount of air pockets or pores that can occur while curing.

APPLICATIONS

The main intent of this research is to eventually establish an effective “structural health monitoring” system that can detect the health of the bonds without destroying the bonded system. By correlating specific damage/environmental exposures of the bond with the magnetic signatures, this could be a solution to qualify bond health. This technique can be used to detect bonding health states in commercial aircrafts, government aircrafts and vehicles and virtually any system that uses a bonded composite structure.

FURTHER WORK

The continuation of correlating magnetic signatures to bond states will still be performed. More data and scans are needed to effectively see what the magnetic signatures are before environmental exposure and what they are after. Similarly mechanical fatigue samples will also be scanned before and after to have comparisons of magnetic signatures on mechanical loading. Additionally larger MENs on the order or 100nm are being looked into and tested. Due to the larger size, the MENs will be easier to characterize and view in-situ. Larger doping concentrations will also be looked into for sensitivity of magnetic signatures.

As well with doping of the adhesive, it is conceivable that the prepreg matrix can be doped with the MENs. With MENs incorporation into prepreg material, localized damage can be addressed and looked into. Currently, the sample scans are given off as overall or bulk magnetic signatures. Selective scanning of certain regions can identify specific areas of bonded area that are potentially compromised. Determination of localized damage with localized scans will be essential and highly desirable as part of the health monitoring system. Along with localized damage, the degree of cure can also be

determined. Composites are very sensitive when it comes to manufacturing. The quality of the composite is dependent on the quality of the manufacturing process. Depending on how well the composite cures, the surface charge density of the MENs will reflect accordingly to the magnetic signatures. Understanding how the magnetic signatures vary before after curing will provide important data to determine good manufacturing procedures and samples.

Aside from correlation of magnetic signatures to the various bond states, dispersing the MENs into a viscous medium presents a challenge. Due to the particle size, the surface area of the particles is much higher than larger particles sizes and creates a high surface activity. The high surface activity often results in agglomeration of particles. A way to remedy this is in-situ polymerization. In-situ polymerization allows for control of the cure and control of particle agglomerations which is a possible next step in controlling the dispersion process.

SUMMARY

The addition of 1 vol. % MENs in the epoxy based adhesive was successful in providing better bonding strength in the lap-shear samples. Ultimate shear stress or peak loads of the lap-shear were increased by 12% and 13% increase for peak stresses. G_{II} values of the un-doped compared to doped ENF samples provided an 3.6 times lower energy release rate with a stiffer slope. Moreover, preliminary scans of magnetic signatures via VSM provided promising results of different orders of magnitude when comparing the un-doped baseline, doped baseline, and environmental exposed doped adhesive samples. With promising results and ongoing research provides first steps on becoming a SHM system.

REFERENCES

1. "ASM Material Data Sheet." ASM Material Data Sheet. N.p., n.d. Web. 8 Jan. 2016.
2. T800H DATA SHEET (2008): n. pag. Toray Carbon Fibers America, Inc. Toray. Web. 9 Jan. 2016.
3. Davis, Max, and John Tomblin. "Best Practice in Adhesive-Bonded Structures and Repairs." (2007): n. pag. NTIS. Web. 12 Jan. 2016.
4. Fiebig, Manfred. "Revival of the Magnetoelectric Effect." *Journal of Physics D: Applied Physics* J. Phys. D: Appl. Phys. 38.8 (2005): n. pag. Web.
5. Mahajan, Rp, Kk Patankar, Mb Kothale, Sc Chaudhari, VI Mathe, and Sa Patil. "Magnetoelectric Effect in Cobalt Ferrite-barium Titanate Composites and Their Electrical Properties." *Pramana - J Phys* Pramana 58.5-6 (2002): 1115-124. Web.
6. Pankhurst, Q. A., J. Connolly, S. K. Jones, and J. Dobson. "Applications of Magnetic Nanoparticles in Biomedicine." *Journal of Physics D: Applied Physics* J. Phys. D: Appl. Phys. 36.13 (2003): n. pag. Web.
7. Nair, Madhavan, Rakesh Guduru, Ping Liang, Jeongmin Hong, Vidya Sagar, and Sakhrat Khizroev. "Externally Controlled On-demand Release of Anti-HIV Drug Using Magneto-electric Nanoparticles as Carriers." *Nature Communications Nat Comms* 4 (2013): 1707. Web.
8. Yue, Kun, Rakesh Guduru, Jeongmin Hong, Ping Liang, Madhavan Nair, and Sakhrat Khizroev. "Magneto-Electric Nano-Particles for Non-Invasive Brain Stimulation." *PLoS ONE* 7.9 (2012): n. pag. Web.
9. Guduru, Rakesh, Ping Liang, Carolyn Runowicz, Madhavan Nair, Venkata Atluri, and Sakhrat Khizroev. "Magneto-electric Nanoparticles to Enable Field-controlled High-Specificity Drug Delivery to Eradicate Ovarian Cancer Cells." *Sci. Rep. Scientific Reports* 3 (2013): n. pag. Web.
10. Gao, Feng, Xinyi Chen, Kuibo Yin, Shuai Dong, Zhifeng Ren, Fang Yuan, Tao Yu, Zhigang Zou, and Jun-Ming Liu. "Visible-Light Photocatalytic Properties of Weak Magnetic BiFeO₃ Nanoparticles." *ChemInform* 38.49 (2007): n. pag. Web.
11. Saha, J., G. Sharma, S.d. Kaushik, V. Rani, Sudesh, V. Siruguri, and S. Patnaik. "Magneto-electric Coupling in Ca₃CoMnO₆ Thin Films." *Journal of Magnetism and Magnetic Materials* 400 (2016): 282-85. Web.

12. Petcharoen, Karat, and Anuvat Sirivat. "Magneto-electro-responsive Material Based on Magnetite Nanoparticles/polyurethane Composites." *Materials Science and Engineering: C* 61 (2016): 312-23. Web.
13. Hsieh, T.h., A.j. Kinloch, K. Masania, A.c. Taylor, and S. Sprenger. "The Mechanisms and Mechanics of the Toughening of Epoxy Polymers Modified with Silica Nanoparticles." *Polymer* 51.26 (2010): 6284-294. Web.
14. Bray, D.j., P. Dittanet, F.j. Guild, A.j. Kinloch, K. Masania, R.a. Pearson, and A.c. Taylor. "The Modelling of the Toughening of Epoxy Polymers via Silica Nanoparticles: The Effects of Volume Fraction and Particle Size." *Polymer* 54.26 (2013): 7022-032. Web.
15. Brooker, R. D., A. J. Kinloch, and A. C. Taylor. "The Morphology and Fracture Properties of Thermoplastic-Toughened Epoxy Polymers." *The Journal of Adhesion* 86.7 (2010): 726-41. Web.
16. Fu, Shao-Yun, Xi-Qiao Feng, Bernd Lauke, and Yiu-Wing Mai. "Effects of Particle Size, Particle/matrix Interface Adhesion and Particle Loading on Mechanical Properties of Particulate-polymer Composites." *Composites Part B: Engineering* 39.6 (2008): 933-61. Web.
17. Uddin, M. F., H. Mahfuz, S. Zainuddin, and S. Jeelani. "Improving Ballistic Performance of Polyurethane Foam by Nanoparticle Reinforcement." *Journal of Nanotechnology* 2009 (2009): 1-8. Web.
18. Stewart, Justin K., Hassan Mahfuz, and Leif A. Carlsson. "Enhancing Mechanical and Fracture Properties of Sandwich Composites Using Nanoparticle Reinforcement." *J Mater Sci Journal of Materials Science* 45.13 (2010): 3490-496. Web.
19. Rosso, P., L. Ye, K. Friedrich, and S. Sprenger. "A Toughened Epoxy Resin by Silica Nanoparticle Reinforcement." *Journal of Applied Polymer Science J. Appl. Polym. Sci.* 101.2 (2006): 1235-236. Web.
20. Mahrholz, T., J. Stängle, and M. Sinapius. "Quantitation of the Reinforcement Effect of Silica Nanoparticles in Epoxy Resins Used in Liquid Composite Moulding Processes." *Composites Part A: Applied Science and Manufacturing* 40.3 (2009): 235-43. Web.
21. Manjunatha, C.m., A.c. Taylor, A.j. Kinloch, and S. Sprenger. "The Tensile Fatigue Behaviour of a Silica Nanoparticle-modified Glass Fibre Reinforced Epoxy Composite." *Composites Science and Technology* 70.1 (2010): 193-99. Web.

22. Paramsothy, M., J. Chan, R. Kwok, and M. Gupta. "The Effective Reinforcement of Magnesium Alloy ZK60A Using Al₂O₃ Nanoparticles." *Journal of Nanoparticle Research J Nanopart Res* 13.10 (2011): 4855-866. Web.
23. Creton, Costantino, and Eric Papon. "Materials Science of Adhesives: How to Bond Things Together." *MRS Bull. MRS Bulletin* 28.06 (2003): 419-23. Web.
24. Haisma, Jan, and G.A.C.M. Spierings. "Contact Bonding, including Direct-bonding in a Historical and Recent Context of Materials Science and Technology, Physics and Chemistry." *Materials Science and Engineering: R: Reports* 37.1-2 (2002): 1-60. Web.
25. Derks, Didi, Anke Lindner, Costantino Creton, and Daniel Bonn. "Cohesive Failure of Thin Layers of Soft Model Adhesives under Tension." *J. Appl. Phys. Journal of Applied Physics* 93.3 (2003): 1557. Web.
26. "Elementary Fracture Mechanics of Solids." *Theory and Practice Adhesion Measurement Methods* (2005): 155-86. Web.
27. Balzani, C., W. Wagner, D. Wilckens, R. Degenhardt, S. Büsing, and H.-G. Reimerdes. "Adhesive Joints in Composite Laminates—A Combined Numerical/experimental Estimate of Critical Energy Release Rates." *International Journal of Adhesion and Adhesives* (2011): n. pag. Web.
28. Silva, Lucas F. M. Da, T. N. S. S. Rodrigues, M. A. V. Figueiredo, M. F. S. F. De Moura, and J. A. G. Chousal. "Effect of Adhesive Type and Thickness on the Lap Shear Strength." *The Journal of Adhesion* 82.11 (2006): 1091-115. Web.
29. ASTM Standard D5528-13, (2013), "Standard Test Method for Mode I Interlaminar Fracture Toughness of Unidirectional Fiber-Reinforced Polymer Matrix Composites" ASTM International, West Conshohocken, PA, 2013, DOI: 10.1520/D5528-13, www.astm.org
30. ASTM Standard D7905/D7905m-14, (2014), "Standard Test Method for Determination of the Mode II Interlaminar Fracture Toughness of Unidirectional Fiber-Reinforced Polymer Matrix Composites" ASTM International, West Conshohocken, PA, 2014, DOI: 10.1520/D7905_D7905M-14, www.astm.org
31. ASTM Standard D6671/D6671M, (2013), "Standard Test Method for Mixed Mode I-Mode II Interlaminar Fracture Toughness of Unidirectional Fiber Reinforced Polymer Matrix Composites" ASTM International, West Conshohocken, PA, 2013, DOI: 10.1520/D6671_D6671M-13E01, www.astm.org

32. ASTM Standard D5868-01, (2014), “Standard Test Method for Lap Shear Adhesion for Fiber Reinforced Plastic (FRP) Bonding” ASTM International, West Conshohocken, PA, 2014, DOI: 10.1520/D5868-01R14, www.astm.org
33. 3M. Product Selection Guide. St. Paul: 3M, 2014. 3M Science. Applied to Life. 3M Industrial Adhesives & Tapes Division, 2014. Web. 5 Apr. 2016.